

NBSIR 75-772

The Dynamic Response of Helicoid Anemometers

J. M. McMichael and P. S. Klebanoff

Aerodynamics Section
Mechanics Division
Institute for Basic Standards
National Bureau of Standards
Washington, D. C. 20234

November 1975

Final

Prepared for
Federal Highway Administration
Office of Research
Structures and Applied Mechanics Division
Washington, D. C. 20590

NBSIR 75-772

THE DYNAMIC RESPONSE OF HELICOID ANEMOMETERS

J. M. McMichael and P. S. Klebanoff

Aerodynamics Section
Mechanics Division
Institute for Basic Standards
National Bureau of Standards
Washington, D. C. 20234

November 1975

Final

Prepared for
Federal Highway Administration
Office of Research
Structures and Applied Mechanics Division
Washington, D. C. 20590



U.S. DEPARTMENT OF COMMERCE, Rogers C.B. Morton, *Secretary*
James A. Baker, III, *Under Secretary*
Dr. Betsy Ancker-Johnson, *Assistant Secretary for Science and Technology*
NATIONAL BUREAU OF STANDARDS, Ernest Ambler, *Acting Director*

LIST OF SYMBOLS

| | |
|-------------|---------------------------------------------------------------------------------------------------------|
| a | amplitude of velocity square-wave = $\epsilon \frac{\Pi}{4}$ |
| e | base of natural logarithms |
| exp | (subscript) experimental value |
| f | function defined by Equation (13) |
| fps | feet per second |
| i | square-root of minus one |
| k,l,n | summation indices |
| t | time |
| u | dimensionless velocity fluctuation |
| y,z | normalized transverse test-section axes |
| A | constant defined by Equation (7) |
| B | coefficient of bearing friction defined by Equation (2) |
| C_n | Fourier coefficients of periodic velocity fluctuation, defined by Equation (23) |
| $ C_n $ | amplitude of C_n |
| D_n | Fourier coefficients of rotation rate, defined by Equation (34) |
| $ D_n $ | amplitude of D_n |
| $D_n^{(i)}$ | Fourier coefficients of the i^{th} term in the perturbation expansion defined by Equation (25) |
| E | instantaneous voltage output of Gill anemometer system |
| \bar{E} | average value of E |
| E_n | Fourier coefficients of the anemometer voltage, defined by Equation (65) |
| $ E_n $ | amplitude of n^{th} harmonic of the anemometer voltage |
| F | retarding torque on anemometer rotor due to bearing friction |

| | |
|----------------|--------------------------------------------------------------------------------|
| $G(\xi)$ | nondimensional aerodynamic torque defined by Equation (3) |
| I | moment of inertia of anemometer rotor |
| K | meter factor defined by Equation (13) |
| K_1 | anemometer voltage sensitivity defined by Equation (64) |
| L | distance-constant |
| R | characteristic radius of anemometer rotor |
| S | rate of rotation of anemometer rotor |
| S_e | steady flow equilibrium rotation rate |
| S^* | rotation rate defined by Equation (18) |
| \bar{S} | average rate of rotation |
| T | aerodynamic torque on anemometer rotor |
| U | instantaneous air speed |
| \bar{U} | average air speed |
| U_o | constant defined by Equation (14) |
| β | coefficient defined by Equation (11) |
| β_o | coefficient defined by Equation (22) |
| ϵ | fundamental amplitude of velocity fluctuation relative to \bar{U} |
| ϕ_n | phase of n^{th} harmonic of velocity fluctuation |
| ω | angular frequency |
| ρ_a | density of air stream |
| σ | relative fluctuation in rotation rate, Equation (17) |
| $\sigma^{(n)}$ | coefficient of n^{th} term in the perturbation expansion for σ |
| τ | time constant |
| τ_o | time constant defined by Equation (21) |
| ξ | dimensionless rotation rate defined by Equation (4) |
| ξ_o | asymptotic value of ξ as $U \rightarrow \infty$. |

LIST OF FIGURES

1. Characteristic Curve of ξ/ξ_0 as a Function of Flow Speed.
2. Schematic Steady Flow Calibration Curve Defining S^* and σ .
3. Theoretical Over-Registration of Mean Speed.
4. Theoretical Phase Dependence of Ratio of Second Harmonics.
5. Ratio of Second Harmonics with $\phi_2 = 0$.
6. Ratio of Second Harmonics with $\phi_2 = \Pi$.
7. Theoretical Square-Wave Response.
8. Configuration of the Instruments in the Test-Section.
9. Horizontal and Vertical Distributions of Free-Stream Velocity $U_{CL} = 35$ fps.
10. Horizontal Distribution of Free-Stream Longitudinal Turbulence Intensity, $U_{CL} = 35$ fps.
11. Instrumentation for Measured Dynamic Response Characteristics.
12. Domain of Mean Speed and Frequency Used in the Experiments.
13. Domain of Fundamental Amplitude and Frequency Covered by the Experiments.
14. Domain of First and Second Harmonics of the Velocity Fluctuation.
15. Steady Flow Calibration Curve.
16. Attenuation of the Response Fundamental.
17. Comparison of Theoretical and Experimental Values of Response Fundamental Amplitude, Neglecting Bearing Friction.
18. Comparison of Theoretical and Experimental Values of Response Fundamental Amplitude, with Bearing Friction.
19. Comparison of Measured and Predicted Overspeeding Errors.
20. Response of Second Harmonic.

CONTENTS

| | Page |
|---------------------------------------------------------------|------|
| ABSTRACT ----- | 1 |
| 1. INTRODUCTION ----- | 1 |
| 2. ANALYTICAL CONSIDERATIONS ----- | 3 |
| 2.1 Torque Balance ----- | 3 |
| 2.2 The Driving Torque - Dimensional Considerations ----- | 4 |
| 2.3 The Response Equation ----- | 6 |
| 2.4 The Condition of Steady Flow Equilibrium ----- | 7 |
| 2.5 The Dynamic Response Equation ----- | 7 |
| 2.6 The Perturbation Solution for the Dynamic Response ----- | 8 |
| 2.6.1 The Perturbation Expansion ----- | 9 |
| 2.6.2 The Steady-State Solution ----- | 9 |
| 2.6.3 The Over-Registration of Mean Speed ----- | 10 |
| 2.6.4 The Amplitude of the Response Fundamental ----- | 12 |
| 2.6.5 The Amplitude of the Response Second Harmonic ----- | 13 |
| 2.6.6 The Response to a Square-Wave Velocity Fluctuation ---- | 14 |
| 3. EXPERIMENTAL APPARATUS AND PROCEDURE ----- | 17 |
| 3.1 The Apparatus ----- | 17 |
| 3.2 Range of Parameters ----- | 18 |
| 4. EXPERIMENTAL RESULTS ----- | 19 |
| 4.1 The Steady-Flow Response ----- | 19 |
| 4.2 Determining the Distance-Constant ----- | 19 |
| 4.3 The Overspeeding Error ----- | 21 |
| 4.4 The Response Second Harmonic ----- | 22 |
| 5. CONCLUSIONS ----- | 22 |
| 6. ACKNOWLEDGEMENTS ----- | 23 |
| 7. REFERENCES ----- | 23 |

THE DYNAMIC RESPONSE OF HELICOID ANEMOMETERS

J. M. McMichael and P. S. Klebanoff

ABSTRACT

The results of an analytical and experimental investigation of the dynamic response of a helicoid anemometer are presented. The experimental investigation was conducted using the NBS Unsteady Flow Facility and data are presented which illustrate the dynamic behavior in a spatially uniform, fluctuating flow with varying amplitudes, frequencies, and mean velocities. An analytical model governing the dynamic response is also presented and compared with the experimental results.

Key Words: Air; analytical; anemometer; dynamic response; experimental; lag; unsteady flow.

1. INTRODUCTION

The importance of such problems as the effect of wind loading on structures and buildings under the action of a variable wind, turbulent transport processes in the atmosphere as they relate to pollution, the gathering of climatological and weather data, the need to further our understanding of the properties of atmospheric turbulence, etc., has emphasized the necessity of improving the ability of anemometers to provide accurate measurements of variations in wind movement, and to reliably reproduce the true wind speed.

One approach to this problem has been to obtain the necessary information by physical modeling in wind tunnels. Although physical modeling still appears to be a most useful approach for studying under controlled conditions the variety of wind effects that may occur, it has become fully evident that there is a need for full-scale studies. This is particularly true with respect to understanding the effects of wind on structures and buildings, not only to establish the correctness of correlations between full-scale and model tests, but because it is not realistic to expect to simulate in the wind tunnel the lower wave numbers of atmospheric turbulence pertinent to appropriate dynamic modeling. In this connection it would be preferable, if one were limited to wind tunnel modeling, to approach the problem by studying the response of a structure to certain discrete frequencies and stepwise changes in velocity.

It is therefore important that reliable mean velocity and turbulence measurements be made in the field. Mechanical-type instruments such as

rotary anemometers, are the most widely used, and will continue to be the principal instrumentation for gathering field data. Although rotary anemometers were initially conceived primarily for the measurement of mean speeds, the need for atmospheric turbulence data has led increasingly to the application of these instruments for this purpose. An understanding of the dynamic response characteristics of anemometers is therefore essential.

In steady flows rotary anemometers adjust to a rate of rotation such that the aerodynamic forces on the rotor element produce a sufficient driving torque to balance the retarding torques, the latter arising from bearing friction, signal generator resistance, and fluid friction acting on the rotor. In unsteady flows the net torque at any instant produces an angular acceleration of the rotor which depends upon the inertia of the rotor. The mechanical inertia of rotary anemometers leads to an effect termed inertial averaging, where the dynamic response exhibits an attenuation dependent upon frequency, inertia, flow velocity, fluid density and viscosity, and the physical and aerodynamic characteristics of the rotor.

In principal, the dynamic behavior of any rotary anemometer could be predicted from full knowledge of all these factors. However, the detailed aerodynamics of anemometer rotors is imposingly complex, and all theoretical treatments of the problem to date rely upon selected models based upon certain simplifying assumptions and requiring the evaluation of certain empirical constants. Nevertheless, useful information can be extracted from the various models in the form of explicit functional dependence of the response upon the primary independent variables.

All of the theoretical models proposed to date (1-7) reveal that the driving torque is nonlinearly related to the flow velocity. However, the lack of an adequate understanding of the effect this nonlinear behavior has on atmospheric turbulence measurements, in particular on atmospheric turbulence spectra, has limited experimental efforts (8-11) to make such measurements to utilizing linear systems theory and the system transfer function for the linearized response equations to correct for inertial averaging. However, there does appear to be a fundamental reason to question the adequacy of linear assumptions in as much as it is well known that mean flow velocities obtained from rotary anemometers in fluctuating winds characteristically exhibit an over-speeding or over-registration introduced by the nonlinear nature of the dynamic response.

Since the pioneering experimental research of Schubauer and Adams (1) established that the time constant for rotary anemometers varies inversely with the flow speed, it has been common practice to characterize the dynamic response of rotary anemometers in a simple wind tunnel test by determining the "distance-constant" using the "locked-rotor" technique. In this method the rotor is released from rest in a steady flow and the time-constant of the exponential rise in its rotation rate towards its equilibrium value is determined, which together with the flow velocity

determines the distance constant. On the other hand very little has been done in studying the dynamic response in controlled fluctuating flows, and what has been done (2,4,12) has been confined to the phenomenon of over-speeding and its dependence upon the velocity amplitude and frequency with no attention being given to the higher harmonics of the fluctuations in the anemometer response.

In the present report the results of wind tunnel tests of the dynamic response of a Gill helicoid anemometer, Model 27002,* conducted in the NBS Unsteady Flow Facility over a range of known frequencies, amplitudes, and mean velocities are presented. The primary purpose is to determine to what extent the linear system transfer function adequately represents the observed response, and to what extent, if any, the inherent nonlinearities of a helicoid anemometer may affect the response.

In addition to the experiments, a dynamic response equation which is believed to be applicable to rotary anemometers of various types is presented. The equation exhibits the essential nonlinearity which is inherent in all rotary anemometers, but Reynolds number effects are neglected although the retarding torque due to bearing friction and signal generator resistance is incorporated into the model presented.

An approximate solution based upon a second-order perturbation expansion is presented for the nonlinear dynamic response to arbitrary periodic flows. Expressions for the over-speeding error and the response harmonics are compared with the experimental results.

Dimensional quantities throughout this report are expressed in engineering units which are customarily used in this field.

2. ANALYTICAL CONSIDERATIONS

2.1 Torque Balance

The general torque balance for rotary anemometers may be written

$$I \frac{dS}{dt} = T - F \quad (1)$$

where I is the moment of inertia of the rotor, S is the instantaneous angular velocity, t is time, T is the driving torque, and F is the retarding torque.

It is assumed at the outset that aerodynamic friction may be neglected. The remaining retarding torques arise from bearing friction and signal gen-

*This particular instrument was selected as being representative of a given class of rotary anemometers and this selection does not represent an endorsement.

erator resistance, and it is assumed that these may be combined and expressed as follows:

$$F = BS , \quad (2)$$

where B is a constant resistance coefficient. This relation should suffice for lubricated bearings, including the effective resistance of the signal generator, and has been employed by Onuma (13). Starting friction is ignored since attention shall be restricted to air speeds in excess of the starting speed.

Many expressions for the driving torque have appeared in the literature (1-7) with varying degrees of sophistication depending upon the particular model adopted for the aerodynamic forces on the rotor. Some of the models account for Reynolds number effects while others simply proceed from dimensional arguments and the assumption of frictionless flow. However, all of the models indicate that the driving torque is nonlinearly related to the flow velocity, and it is this aspect upon which the following analysis is focused.

2.2 The Driving Torque - Dimensional Considerations

The view has been expressed by Onuma (13) and Jepson (2), among others, that both cup and propeller-type anemometers obey the same general response equations. The plausibility of this contention may be established from dimensional considerations.

For frictionless flow the driving torque must depend only upon the following variables:

$$T = T(\rho_a, U, S, R)$$

where ρ_a is the fluid density, R is a length characteristic of the physical dimensions of the rotor, and U is the instantaneous air speed. The flow about the rotor is assumed quasi-steady so that T is independent of the time derivatives of U. In nondimensional terms

$$\frac{T}{\rho_a U^2 R^3} = G(\xi) , \quad (3)$$

where

$$\xi = \frac{RS}{U} . \quad (4)$$

To develop an expression for G(ξ), one proceeds from the observation that the steady flow calibration curve (see for example Figure (15)) for rotary anemometers approaches a straight line as U increases. This means that the calibration data, when ξ is plotted as a function of U, character-

istically exhibits the form indicated in Figure 1. As U increases ξ asymptotically approaches a constant value ξ_0 , which is simply related to the meter factor K ,

$$\xi_0 = RK$$

In steady flow without friction, $T = 0$ and $\xi = \xi_0$ over the entire range of U . It follows that $G(\xi_0) = 0$. When friction is present or when the flow fluctuates a driving torque is produced by departures of ξ from ξ_0 , and a Taylor series expansion may be written for $G(\xi)$ as follows;

$$G(\xi) = \left. \frac{\partial G}{\partial \xi} \right|_{\xi_0} (\xi - \xi_0) + \left. \frac{\partial^2 G}{\partial \xi^2} \right|_{\xi_0} \frac{(\xi - \xi_0)^2}{2} + \dots \quad (5)$$

provided that the derivatives are continuous.

To lowest order then, the driving torque may be written

$$T = A U^2 \left(K - \frac{S}{U} \right) \quad (6)$$

where

$$A = \rho_a R^4 \left(- \left. \frac{\partial G}{\partial \xi} \right|_{\xi_0} \right) \quad (7)$$

is a positive constant. Equation (6) contains the inherent nonlinearity in the flow speed to which the overspeeding known to occur in all rotary anemometers may be attributed. The effect of this nonlinearity on anemometer response in unsteady flows is explored in subsequent sections of this report.

In support of the differentiability assumed above it may be noted that the resulting expression for the driving torque (Equation (6)) is identical in form to the expression obtained empirically by Ower (4), the expression obtained from momentum arguments by Rubin, et al. (3), and the expressions obtained from airfoil analysis by Rubin, et al. (3) and by Jepson (2), neglecting aerodynamic friction. The advantage of the more elaborate models, of course, is that the dependence of the aerodynamic driving torque upon rotor geometry and aerodynamic characteristics is more explicit. Nevertheless, these models still require the experimental evaluation of aerodynamic force coefficients, and there is no loss of generality by adopting Equation (6) and regarding A as an empirical constant to be determined.

While retaining only the lowest order term in the above expansion would suggest that the resulting torque expression is limited to modest

departures of ξ from ξ_0 , this assumption appears to be no more restrictive than the assumption of modest angles of attack for the rotor blades which underlies the models adopted by Jepson (2) and Rubin, et al. (3).

2.3 The Response Equation

Substitution of Equations (2) and (6) into Equation (1) yields the following response equation

$$\frac{I}{A} \frac{dS}{dt} + \left(U + \frac{B}{A}\right)S = KU^2, \quad (8)$$

where K is defined by Equation (13).

In the case of a step change in U at time t_0 the response equation may be written

$$\tau \frac{dS}{dt} + (1 + \beta)S = KU, \quad (9)$$

where the "time-constant" τ is defined by

$$\tau = \frac{I}{AU} \quad (10)$$

and

$$\beta = \frac{B}{AU}. \quad (11)$$

U is understood to be the constant flow speed for $t > t_0$. Neglecting friction, it is clear that the exponential response in this case is characterized by a time-constant which varies inversely with the flow velocity, and that the product

$$L = \tau U = \frac{I}{A} \quad (12)$$

is a constant. L has been termed the "distance-constant" by Schubauer and Adams (1) who, having obtained Equation (12) empirically, deduced the form of Equation (8) (without friction) by assuming the driving torque to be proportional to $(KU - S)$, the departure of the rotation rate from its frictionless equilibrium value.

The time constant of the transient response including bearing friction is given by

$$\tau' = \frac{L}{U + \frac{B}{A}},$$

which implies that L as determined by the locked-rotor technique and Equation (12) may be slightly in error unless B/A is sufficiently small compared to U. For example, in the wind tunnel tests described in detail in later sections of this report it was found that B/A \approx 1 fps so that if U = 10 fps in a locked rotor test a 10 percent error in L would result unless the results were corrected as indicated by the above equation.

2.4 The Condition of Steady Flow Equilibrium

When the flow velocity U is held constant, the rotation rate reaches an equilibrium value S_e such that $dS/dt = 0$. Applying this condition to Equation (8) it follows that

$$S_e = \frac{KU^2}{U + \frac{B}{A}} \equiv f(U) . \quad (13)$$

As U increases the calibration curve, S (U) becomes a straight line of slope K (see Figure (15)). The equation of this straight line asymptote may be expressed as

$$S_e = K(U - U_o) , \quad (14)$$

where U_o is the velocity intercept when $S_e = 0$. For large values of U such that B/AU \ll 1, Equation (13) is approximated by

$$S_e \approx KU(1 - \frac{B}{AU}) .$$

Comparing this to Equation (14) it follows that

$$U_o = \frac{B}{A} \quad (15)$$

Thus two of the three coefficients in Equation (8) may be determined for a given anemometer by a simple steady flow calibration. The remaining coefficient is the distance-constant which must be determined dynamically.

2.5 The Dynamic Response Equation

When Equations (12) and (15) are substituted into Equation (8) the latter may be written

$$L \frac{dS}{dt} + (U + U_o)S = KU^2 . \quad (16)$$

While Equation (16) is a linear first-order equation with non-constant coefficients, the response S is nonlinear in the sense that if $S_1(t)$ is a solution when $U = U_1(t)$, and $S_2(t)$ is a solution when $U = U_2(t)$, then

$S_1 + S_2$ is not a solution when $U = U_1 + U_2$.

Direct integration of the equation is possible in principal for arbitrary functions of time, $U(t)$. The exact integration has been presented by Onuma (13) in the case of a purely sinusoidal velocity fluctuation about some mean value.

Solutions for the case of arbitrary periodic velocity fluctuations have not appeared in the literature heretofore. In order to develop an approximate solution in this case it is convenient to express Equation (16) in terms of the variable σ defined by the following equation:

$$S = S^*(1 + \sigma) \quad (17)$$

where S^* is given by

$$S^* = f(\bar{U}) \quad (18)$$

and f is defined by Equation (13). These definitions are illustrated graphically in Figure 2. The instantaneous velocity may be expressed as

$$U = \bar{U}(1 + u) \quad (19)$$

where \bar{U} is the temporal mean flow velocity, and u is the relative velocity fluctuation.

Substitution of Equations (13), (17), (18), and (19) into Equation (16) yields the following dimensionless dynamic response equation

$$\tau_o \frac{d\sigma}{dt} + (1 + \beta_o + u)\sigma = (1 + 2\beta_o)u + (1 + \beta_o)u^2, \quad (20)$$

where

$$\tau_o = \frac{L}{\bar{U}}, \quad (21)$$

and

$$\beta_o = \frac{U_o}{\bar{U}}. \quad (22)$$

2.6 The Perturbation Solution for the Dynamic Response

It is noteworthy that there are only two coefficients, β_o and τ_o , in the dynamic response equation which require experimental determination. β_o is obtained with the aid of the steady flow calibration, and τ_o derives from the distance constant obtained in a dynamic calibration. This observation represents a substantially simpler view than that proposed by Wyngaard (5) wherein as many as four torque derivatives must be measured experimentally in addition to the distance constant.

The perturbation solution developed in this section assumes a general periodic velocity fluctuation, and the results obtained are subject to the assumptions that \bar{U} remains different from zero and the relative amplitude of the velocity fluctuation remains less than unity.

2.6.1 The Perturbation Expansion

The magnitude of the velocity fluctuation is characterized by ϵ , the relative amplitude of the fundamental component of the Fourier series expansion

$$u = \frac{\epsilon}{2} \sum_{n=-\infty}^{\infty} C_n e^{in\omega t} \quad (23)$$

where $|C_n|$ is the amplitude of the n^{th} harmonic, ω is the angular frequency, and by definition

$$C_0 = 0 \text{ and } C_1 = 1 . \quad (24)$$

The assumption is made that ϵ is sufficiently small that σ may be expanded in a power series as follows:

$$\sigma = \sigma^{(0)} + \epsilon\sigma^{(1)} + \epsilon^2\sigma^{(2)} + \dots \quad (25)$$

Substitution of this expression into Equation (20), recognizing that u is of order ϵ , leads to the following hierarchy of equations for $\sigma^{(n)}$:

$$\tau_0 \frac{d\sigma^{(0)}}{dt} + (1 + \beta_0)\sigma^{(0)} = 0 , \quad (26)$$

$$\tau_0 \frac{d\sigma^{(1)}}{dt} + (1 + \beta_0)\sigma^{(1)} = (1 + 2\beta_0) \frac{u}{\epsilon} - \sigma^{(0)} \frac{u}{\epsilon} , \quad (27)$$

$$\tau_0 \frac{d\sigma^{(2)}}{dt} + (1 + \beta_0)\sigma^{(2)} = (1 + \beta_0) \left(\frac{u}{\epsilon}\right)^2 - \sigma^{(1)} \frac{u}{\epsilon} \quad (28)$$

and so on. The solution is sought through second order only.

2.6.2 The Steady-State Solution

Equation (26) has the trivial steady-state solution

$$\sigma^{(0)} = 0 \quad (29)$$

The Fourier series expansion for $\sigma^{(1)}$ may be written

$$\sigma^{(1)} = \frac{1}{2} \sum_{n=-\infty}^{\infty} D_n^{(1)} e^{in\omega t} \quad (30)$$

Substituting Equations (23) and (30) into Equation (27), and equating coefficients for each value of n , one obtains

$$D_n^{(1)} = \frac{(1 + 2\beta_o)C_n}{(1 + \beta_o) + in\omega\tau_o} \quad (31)$$

Similarly, the Fourier series expansion for $\sigma^{(2)}$ is

$$\sigma^{(2)} = \frac{1}{2} \sum_{n=-\infty}^{\infty} D_n^{(2)} e^{in\omega t} \quad (32)$$

The left side of Equation (28) becomes

$$\frac{1}{2} \sum_{\ell=-\infty}^{\infty} \sum_{k=-\infty}^{\infty} \frac{C_{\ell}}{2} [(1 + \beta_o)C_k - D_k^{(1)}] e^{i(k + \ell)\omega t}$$

Equating coefficients such that $n = k + \ell$ leads to the result:

$$D_n^{(2)} = \frac{1}{2} \sum_{k=-\infty}^{\infty} \frac{C_{n-k} [(1 + \beta_o)C_k - D_k^{(1)}]}{(1 + \beta_o) + in\omega\tau_o} \quad (33)$$

Substituting Equations (29) through (33) into Equation (25) yields the second-order solution for σ :

$$\sigma = \frac{\epsilon}{2} \sum_{n=-\infty}^{\infty} D_n e^{in\omega t}, \quad (34)$$

where

$$D_n = \frac{1}{(1 + \beta_o) + in\omega\tau_o} \left\{ (1 + 2\beta_o)C_n + \frac{\epsilon}{2} \sum_{k=-\infty}^{\infty} C_k C_{n-k} - k \left[(1 + \beta_o) - \frac{(1 + 2\beta_o)}{(1 + \beta_o) + ik\omega\tau_o} \right] \right\} \quad (35)$$

In the following paragraphs this solution is examined for the overspeeding error, the response fundamental and the response second harmonic. These expressions are compared to the experimental results in Section 4 of this report. The theoretical response to a square-wave velocity fluctuation is also discussed below.

2.6.3 The Over-Registration of Mean Speed

The mean value of the response, denoted $\bar{\sigma}$, is obtained quite simply from the term in Equation (34) corresponding to $n = 0$,

$$\bar{\sigma} = \frac{\epsilon}{2} D_0 \quad (36)$$

where, from Equation (35) and (24), D_o is given by

$$D_o = \frac{\epsilon}{2} \sum_{k=-\infty}^{\infty} C_k C_{-k} \left[1 - \frac{1 + 2\beta_o}{(1 + \beta_o) + ik\omega\tau_o} \right].$$

Observing that because u must be real $C_{-k} = C_k^*$, the conjugate of C_k , and by pairing corresponding positive and negative values of k in the sum above, $\bar{\sigma}$ may be written

$$\bar{\sigma} = \frac{\epsilon^2}{2} \sum_{k=1}^{\infty} |C_k|^2 \left[1 - \frac{1 + 2\beta_o}{(1 + \beta_o)^2 + (k\omega\tau_o)^2} \right] \quad (37)$$

In the case of a pure sinusoidal velocity fluctuation $C_1 = 1$ and $C_k = 0$ for $k > 1$, reducing Equation (37) to

$$\bar{\sigma} = \frac{\epsilon^2}{2} \left[1 - \frac{1 + 2\beta_o}{(1 + \beta_o)^2 + (\omega\tau_o)^2} \right]. \quad (38)$$

The exact expression for $\bar{\sigma}$ obtained by Onuma (13) in this case may be reduced to Equation (38) by assuming that the amplitude of the velocity fluctuation is small compared to the mean velocity.

When friction is negligible, $\beta_o \rightarrow 0$, and Equation (38) becomes

$$\bar{\sigma} = \frac{\epsilon^2}{2} \frac{(\omega\tau_o)^2}{1 + (\omega\tau_o)^2}. \quad (39)$$

To illustrate the dependence of the overspeeding error upon ϵ and $\omega\tau_o$, $\bar{\sigma}$, as given by Equation (39), is plotted as a function of ϵ in Figure 3 with $\omega\tau_o$ as a parameter. At high frequencies the maximum possible error is $\epsilon^2/2$.

In order to compare measured values of the mean rotation to those given by this solution, Equations (17) and (18) are averaged and combined to yield

$$\bar{S} = K \bar{U} \frac{(1 + \bar{\sigma})}{(1 + \beta_o)} \quad (40)$$

By measuring the true mean speed, \bar{U} , knowing the distance constant and the steady flow calibration intercept, the values of \bar{S} predicted by Equations (37) and (40) can be computed and compared to the measured values presented in Section 4.

2.6.4 The Amplitude of the Response Fundamental

From Equation (35) the magnitude of the response fundamental relative to the input fundamental can be written

$$\left| \frac{D_1}{C_1} \right| = \frac{(1 + 2\beta_0)}{\sqrt{(1 + \beta_0)^2 + (\omega\tau_0)^2}} \left| 1 + \frac{\varepsilon}{2} \sum_{k=-\infty}^{\infty} C_k C_{1-k} - k \left[\frac{1 + \beta_0}{1 + 2\beta_0} - \frac{1}{(1 + \beta_0) + ik\omega\tau_0} \right] \right| \quad (41)$$

If the disturbance amplitude ε is sufficiently small the summation may be neglected leaving only the simple linear first-order transfer function as given by the factor outside the absolute value symbols. For larger values of ε contributions to the response fundamental amplitude arise from the second and higher harmonic amplitudes of the velocity fluctuation. However, these contributions remain small so long as these input higher harmonics remain small compared to unity.

To estimate the degree to which the linear first-order transfer function suffices to describe the response fundamental amplitude, consider that

$$\left| \frac{1 + \beta_0}{1 + 2\beta_0} - \frac{1}{(1 + \beta_0) + ik\omega\tau_0} \right| \leq 2 \text{ for all } k.$$

This is so because β_0 is always positive. It follows that

$$\left| \frac{D_1}{C_1} \right| \leq \frac{1 + 2\beta_0}{\sqrt{(1 + \beta_0)^2 + (\omega\tau_0)^2}} \left[1 + \varepsilon \sum_{k=-\infty}^{\infty} |C_k C_{1-k}| \right]$$

Suppose that, as is the case for the experiments, $C_k \approx 0$ for $k > 2$. The correction term, i.e., the summation term, may be written

$$\varepsilon \sum_{k=-\infty}^{\infty} |C_k C_{1-k}| = 2 \varepsilon |C_2|$$

Hence, as long as the input second harmonic amplitude, $\varepsilon |C_2|$, remains small compared to unity the linear first-order transfer function adequately approximates the attenuation of the response fundamental. Thus,

$$\left| \frac{D_1}{C_1} \right| \approx \frac{1 + 2\beta_0}{\sqrt{(1 + \beta_0)^2 + (\omega\tau_0)^2}} \quad (42)$$

Furthermore, when $\beta_0 \ll 1$ the first-order transfer function may be written

$$\left| \frac{D_1}{C_1} \right| \approx \frac{1}{\sqrt{1 + (\omega\tau_0)^2}} \quad (43)$$

This curve is shown in Figure (16) along with the measured values of the transfer function.

2.6.5 The Amplitude of the Response Second Harmonic

The transfer function for the response second harmonic is quite different from that of the fundamental. In the general situation where the velocity fluctuation contains a second harmonic, the response second harmonic is not given by the linear first-order transfer function which suffices for the fundamental. Rather, the response second harmonic is quite sensitive to the input fundamental as well, and even in the absence of an input second harmonic the nonlinear nature of the response is such that a response second harmonic is generated by the input fundamental. This can be demonstrated by the solution given by Equations (34) and (35) in the following way. First, one may write for the magnitude of the second harmonic

$$|D_2| = \frac{1 + 2\beta_o}{\sqrt{(1 + \beta_o)^2 + (2\omega\tau_o)^2}} \left| C_2 + \frac{\epsilon}{2} \sum_{k=-\infty}^{\infty} C_k C_{2-k} - k \left[\frac{1 + \beta_o}{1 + 2\beta_o} - \frac{1}{(1 + \beta_o) + i k \omega \tau_o} \right] \right| .$$

Again, the linear first-order transfer function has been factored outside the absolute value symbols. The summation term is not generally negligible. Assuming as before that $C_k = 0$ for $k > 2$, the summation may be reduced to

$$\frac{\epsilon}{2} \left[\frac{1 + \beta_o}{1 + 2\beta_o} - \frac{1}{(1 + \beta_o) + i \omega \tau_o} \right] ,$$

since $C_0 = 0$ and $C_1 = 1$ by definition. It follows that

$$|D_2| = \frac{1 + 2\beta_o}{\sqrt{(1 + \beta_o)^2 + (2\omega\tau_o)^2}} \left| C_2 + \frac{\epsilon}{2} \left[\frac{1 + \beta_o}{1 + 2\beta_o} - \frac{1}{(1 + \beta_o) + i \omega \tau_o} \right] \right| . \quad (45)$$

The Fourier coefficient C_2 is complex so that the phase of the second harmonic of the velocity fluctuation may be important in determining the amplitude and phase of the response second harmonic. To illustrate the effect of this phase angle consider Equation (45) in the case where β_o vanishes:

$$|D_2| = \frac{1}{\sqrt{1 + (2\omega\tau_o)^2}} \left| C_2 + \frac{\epsilon}{2} \frac{i\omega\tau_o}{1 + i\omega\tau_o} \right| . \quad (46)$$

To define the phase angle, the velocity fluctuation may be represented by a Fourier sine series:

$$u = \epsilon \sum_{n=1}^{\infty} |C_n| \sin(n\omega t + \phi_n) . \quad (47)$$

The phase of the fundamental, ϕ , is zero by definition. Comparison of Equations (23) and (47) shows that

$$C_2 = |C_2| (\sin \phi_2 - i \cos \phi_2) . \quad (48)$$

Substitution of this expression into Equation (46) leads to the following:

$$|D_2| = \frac{1}{\sqrt{1 + (2\omega\tau_o)^2}} \left[|C_2|^2 + \frac{\epsilon |C_2| \omega\tau_o}{1 + (\omega\tau_o)^2} (\omega\tau_o \sin \phi_2 - \cos \phi_2) + \left(\frac{\epsilon}{2}\right)^2 \frac{(\omega\tau_o)^2}{1 + (\omega\tau_o)^2} \right]^{1/2} \quad (49)$$

In the special case where the velocity fluctuation is purely sinusoidal this reduces to

$$|D_2| = \frac{\epsilon}{2} \frac{1}{\sqrt{1 + (2\omega\tau_o)^2}} \frac{\omega\tau_o}{\sqrt{1 + (\omega\tau_o)^2}} \quad (50)$$

In the more general case, as in the experiments reported in Section 4, C_2 does not vanish, and the transfer function becomes

$$\left| \frac{D_2}{C_2} \right| = \frac{1}{\sqrt{1 + (2\omega\tau_o)^2}} \left[1 + \frac{\epsilon}{|C_2|} \frac{\omega\tau_o}{1 + (\omega\tau_o)^2} (\omega\tau_o \sin \phi_2 - \cos \phi_2) + \frac{1}{4} \left(\frac{\epsilon}{|C_2|}\right)^2 \frac{(\omega\tau_o)^2}{1 + (\omega\tau_o)^2} \right]^{1/2} . \quad (51)$$

The factor outside the braces is the linear first-order transfer function. Clearly, this suffices to describe the attenuation of the second harmonic only when either $\omega\tau_o$ is sufficiently small or the parameter $\epsilon/|C_2|$ is sufficiently small. In either case the transfer function depends only upon the single parameter $\omega\tau_o$. Otherwise, Equation (51) shows that the transfer function is dependent upon three parameters, $\omega\tau_o$, $\epsilon/|C_2|$, and the phase angle ϕ_2 . This observation raises considerable doubt as to the adequacy of the use of the linear first-order transfer function for the correction of atmospheric turbulence spectra as is currently widespread practice.

The transfer function given by Equation (51) is plotted in Figure (4) with $\epsilon/|C_2| = 10$ for phase angles of $0, \pm \Pi/2$, and Π . For any given value of $\omega\tau_o$ phase angles can be found which produce a maximum and a minimum value of the transfer function. Envelopes of these maxima and minima are also shown. It is interesting that the response second harmonic is suppressed strongly for a particular combination of phase and frequency for a given value of $\epsilon/|C_2|$. Furthermore, for values of $2\omega\tau_o$ greater than a certain value (dependent upon $\epsilon/|C_2|$) the response second harmonic is amplified above that predicted by the linear transfer function for all phase angles.

Figures (5) and (6) show the dependence of the transfer function upon the parameter $\epsilon/|C_2|$ for phase angles of 0 and Π , respectively.

Because such significant harmonic distortions as indicated in Figures (4), (5), and (6) are predicted by the perturbation solution, a comparison of this solution with an exact solution for the case of a square-wave velocity fluctuation, where the harmonics are large, is warranted in order to lend credence to the predictions of the theory.

2.6.6 The Response to a Square-Wave Velocity Fluctuation

The velocity fluctuation is represented by a Fourier series as expressed in Equation (23). For a square-wave the Fourier coefficients are given by:

$$C_n = \left\{ \begin{array}{l} -\frac{i}{n}, \text{ for } n \text{ odd} \\ 0, \text{ for } n \text{ even} \end{array} \right\} \quad (52)$$

The amplitude of the square wave is $\pi/4 \epsilon$. Setting β_0 equal to zero for simplicity, the Fourier coefficients for the response are obtained by substituting Equation (52) into Equation (35) with the result

$$D_n = \left\{ \begin{array}{l} -\frac{i}{n} \frac{1}{1 + in\omega\tau_0}, \text{ for } n \text{ odd} \\ -\frac{\epsilon}{2} \frac{1}{1 + in\omega\tau_0} \sum_{\substack{k = -\infty \\ \text{odd}}}^{\infty} \frac{1}{k(n-k)} \frac{i k \omega \tau_0}{1 + i k \omega \tau_0}, \text{ } n \text{ even.} \end{array} \right\} \quad (53)$$

Interestingly, the odd harmonics of the response are given by the linear transfer function while the even harmonics are produced by the nonlinear nature of the response even though the velocity fluctuation in this case contains no even harmonics.

The overspeeding error in this case can be shown to be

$$\bar{\sigma} = \frac{\epsilon^2}{2} \sum_{\substack{k = -\infty \\ \text{odd}}}^{\infty} \frac{(\omega\tau_0)^2}{1 + (k\omega\tau_0)^2}. \quad (54)$$

To determine the exact steady-state solution to Equation (20) in this case consider Figure (7) which shows the response σ in comparison with the velocity fluctuation in the steady state. The velocity fluctuation may be written

$$u = \left\{ \begin{array}{l} \epsilon \frac{\pi}{4}, \text{ for } 0 < \omega(t - t_1) < \pi \\ -\epsilon \frac{\pi}{4}, \text{ for } \pi < \omega(t - t_1) < 2\pi \end{array} \right\} \quad (55)$$

where t_1 is arbitrary. Considering each half-cycle separately Equation (20) may be written

$$\tau_o \frac{d\sigma}{dt} + (1+a)\sigma = (1+a)a, \quad 0 < \omega(t - t_1) < \Pi, \quad (56)$$

$$\tau_o \frac{d\sigma}{dt} + (1+a)\sigma = -(1-a)a, \quad \Pi < \omega(t - t_1) < 2\Pi$$

where $a = \epsilon \Pi/4$. The corresponding initial conditions are

$$\sigma = \left\{ \begin{array}{l} \sigma_1, \quad \omega(t - t_1) = 0 \\ \sigma_2, \quad \omega(t - t_1) = \Pi \\ \sigma_3, \quad \omega(t - t_1) = 2\Pi \end{array} \right\} \quad (57)$$

The condition that the steady-state exists requires that

$$\sigma_3 = \sigma_1 \quad (58)$$

The solution for each half-cycle may be simply written as follows:

$$\sigma = \left\{ \begin{array}{l} a + (\sigma_1 - a)e^{-\frac{(t - t_1)}{\tau_o}(1+a)}, \quad 0 < \omega(t - t_1) < \Pi \\ -a + (\sigma_2 + a)e^{-\frac{[t - (t_1 + \frac{\Pi}{\omega})]}{\tau_o}(1-a)}, \quad \Pi < \omega(t - t_1) < 2\Pi \end{array} \right\} \quad (59)$$

To complete the solution, values for σ_1 and σ_2 must be found. From the above equations one may evaluate σ_2 and σ_3 , respectively:

$$\sigma_2 = a + (\sigma_1 - a)e^{-\frac{\Pi}{\omega\tau_o}(1+a)} \quad (60)$$

and

$$\sigma_3 = -a + (\sigma_2 + a)e^{-\frac{\Pi}{\omega\tau_o}(1-a)} \quad (61)$$

From Equations (58), (60), and (61) one obtains

$$\sigma_1 = \epsilon \frac{\Pi}{4} \frac{e^{(\frac{\epsilon \Pi}{4})(\frac{\Pi}{\omega\tau_o})} - \cosh(\frac{\Pi}{\omega\tau_o})}{\sinh(\frac{\Pi}{\omega\tau_o})}, \quad (62)$$

and σ_2 may be obtained from Equation (60).

The exact solution is plotted relative to the square-wave in Figure (7) along with the perturbation solution for the case where the velocity fluctuation is twenty-five percent of the mean speed $\epsilon = 1/4$, and the frequency is such that $\omega_0 = 1$. The perturbation solution as shown represents a close approximation to the exact solution.

By taking the average value of the exact solution over a complete cycle the overspeeding error can be obtained. In the case shown in Figure (7) one finds $\bar{\sigma}/\epsilon = 0.196$. From Equation (54) one finds that $\bar{\sigma}/\epsilon = 0.180$, in reasonably good agreement.

3. EXPERIMENTAL APPARATUS AND PROCEDURE

3.1 The Apparatus

The experimental measurements were conducted in air in the NBS Unsteady Flow Facility. The instrument studied was a Gill helicoid anemometer, Model 27002 equipped with four-bladed polystyrene propellers, six inches in diameter. The anemometer was mounted centrally in the wind-tunnel test-section with the U sensor aligned to the flow as shown in Figure (8), the V sensor was directed vertically upward, and the W sensor was removed because of spatial limitations in the test section.

The test-section was 4.5 ft square and 16 ft in length. Profiles of mean velocity as measured with a Pitot-static tube in the horizontal and vertical directions are shown in Figure (9) for a centerline mean speed of 35 feet per second. Figure (10) shows the distribution of free-stream turbulent intensity in the horizontal direction. The centerline turbulent intensity varies with mean speed, ranging from 0.2 percent at 10 fps down to 0.08 percent at 40 fps. These data correspond to nominally steady flow.

Figure (8) indicates the location of the Pitot-static tube used to calibrate the hot-wire anemometer, the location of which in proximity to the helicoid anemometer is also indicated. All three instruments were mounted essentially in a horizontal plane as shown. The location of the three instruments with respect to the velocity and intensity profiles is also indicated in Figures (9) and (10).

The electronic instrumentation was arranged as shown in Figure (11). The signals from both the hot-wire system and the Gill anemometer were processed in the same manner with the same instruments, a DC voltmeter, and a Spectral Dynamics Model SD301D Real Time Spectral Analyser* for the measurement of the amplitudes of the Fourier components. The analyser was D.C. coupled to permit measurements at fundamental frequencies down

* Brand names of equipment are used solely to provide a reference for performance characteristics and do not represent an endorsement.

to 0.2 Hz and this necessitated the use of a DC voltage bucking circuit as shown in the figure. All measurements were performed in real time. The frequency resolution was ± 0.01 Hz.

The hot-wire system consisted of a platinum wire 0.040 inches in length with a diameter of 0.0001 inches, operated in a linearized constant-temperature mode. Thermal rise in the air stream of approximately 1.0 °C per hour presented some problems with changes in the hot-wire sensitivity during the experimental runs. This problem was minimized by operating the hot-wire at an overheat of approximately 100 percent, restricting run time to less than two hours, and calibrating before and after each run, using an average of the calibrations in the data reduction. Errors introduced by this thermal drift are estimated at \pm three percent for the mean velocities and \pm one percent for the measured harmonic amplitudes.

3.2 Range of Parameters

The dynamic characteristics of the wind tunnel are presented in detail in a subsequent report. The facility was used to generate periodic axial flow pulsations over a range of mean speeds and fundamental frequencies. The relative fluctuation amplitude was also varied. The harmonic content of the velocity fluctuations varied as well. The primary independent experimental parameters are \bar{U} , $\omega/2\pi$, and ϵ . The harmonic amplitudes and phases of the velocity fluctuation may be regarded as secondary parameters. The range of mean speeds and fundamental frequencies studied is shown in Figure (12). This information is also presented in tabular form in Table 1.

In addition, as revealed in Section 2 of this report, two particular instrument properties (not varied in this study) also determine the response. These are the distance constant, L , and the velocity intercept U_o . Consequently, the response is dependent upon the following three primary dimensionless groups:

$$\beta_o = \frac{U_o}{\bar{U}}, \quad \omega\tau_o = \omega \frac{L}{\bar{U}}, \quad \epsilon. \quad (63)$$

Of secondary importance are the dimensionless Fourier coefficients, C_n , where $n = 2, 3, \dots$ which characterize the amplitudes and phases of the harmonics of the velocity fluctuation.

It should be noted at this point that both the intercept of the linearly extrapolated steady-flow calibration curve, U_o , which reflects the effect of bearing friction in the anemometer, and the distance constant, L , are inversely proportional to the density of the air stream through the quantity A (Equation (7)), and a simple correction can be made to both L and U_o when the anemometer is used in streams of different densities. The density of the air stream in the present study was held to a value of $\rho_a = .0704$ lbm/ft³ with a maximum variation of \pm one percent. This variation arises from variations in stream temperature and pressure.

In terms of nondimensional quantities the range of fluctuation amplitudes and frequencies is shown in Figure (13) and tabulated in Table 1. Fluctuation levels up to approximately 75 percent of the mean speed were studied.

While the harmonics are secondary in terms of their effects on the value determined for the distance constant, they are important in determining the higher harmonics of the response. The range of the second harmonic amplitude relative to the fundamental amplitude is tabulated in Table 1 and shown in Figure (14) as a function of the fundamental amplitude. Values range up to about 40 percent. The third harmonic in all cases was less than 10 percent of the second harmonic and is neglected throughout along with all higher harmonics.

4. EXPERIMENTAL RESULTS

4.1 The Steady-Flow Response

The voltage, E , obtained from the helicoid anemometer under steady conditions is plotted as a function of the speed, U , in Figure (15). The data shown were accumulated under steady flow conditions during the calibrations of the hot-wire anemometer before and after each set of runs on the dynamic response characteristics. The spread of the data in this figure is due primarily to variations in air stream density as discussed in Section 5. Were there no bearing friction, no sensitivity to density would be present and the steady-flow response would be purely kinematic. A least squares straight-line fit of the data produces a velocity intercept of $U_0 = 0.851$ fps.

4.2 Determining the Distance-Constant

According to the model developed in Section 2, all that remains to "calibrate" the anemometer for its dynamic response characteristics is to determine the distance-constant. The model indicates that a sinusoidal frequency response test where the velocity fluctuation is free of harmonics should produce a linear first-order transfer function for the response fundamental as represented by Equation (42) with friction present, or by Equation (43) in the absence of friction. It was argued in Section 2 that the effect of the second harmonic of the velocity fluctuation upon this transfer function should be small as long as the second harmonic amplitude is small relative to the mean velocity. Values of the ratio of the amplitude of the second harmonic to the mean velocity are tabulated in Table 1 along with all of the experimental data presented in this section. This ratio is less than 23 percent for all of the data, and less than 10 percent for the most part. Accordingly, the distance-constant was determined by neglecting the contribution of the harmonics.

The Gill anemometer produces a voltage proportional to the rotation rate:

$$S = K_1 E , \quad (64)$$

where K_1 contains the amplifier gain and the signal generator sensitivity. The spectrum of the signal from the anemometer under steady flow conditions was observed to contain sharp peaks at frequencies corresponding to five and ten times the rotation rate. In performing the experiments care was taken so that frequency components of the velocity fluctuation were not confused with these two frequencies generated by the rotating coil system in the anemometer signal generator.

The Fourier series representation of the anemometer signal may be written

$$E = \frac{1}{2} \sum_{n=-\infty}^{\infty} E_n e^{in\omega t} \quad (65)$$

To compare the harmonic amplitudes, $|E_n|$, with the mathematical model, Equations (64), (65), (34), and (17) may be combined with the result:

$$\frac{K_1}{2} \sum_{n=-\infty}^{\infty} E_n e^{in\omega t} = S^* \left[1 + \frac{\epsilon}{2} \sum_{n=-\infty}^{\infty} D_n e^{in\omega t} \right] \quad (66)$$

It follows that

$$\left| D_1 \right|_{\text{exp}} = \frac{K_1}{\epsilon S^*} |E_1| \quad (67)$$

From this and Equations (13), (18), and (22) one may write

$$\left| D_1 \right|_{\text{exp}} = \frac{K_1}{K\epsilon U} (1 + \beta_0) |E_1| \quad (68)$$

where the subscript "exp" refers to "experimental."

To determine the distance-constant the procedure is as follows. First, β_0 is assumed to be zero as a first approximation. Equation (43) gives the expected transfer function. The experimental values obtained from the measured values of $|E_1|$ and Equation (68) are then plotted as a function of $\omega/2\pi U$ which is proportional to $\omega\tau_0$ as indicated in Equation (63), and a least squares fit of the data to the expression in Equation (43) yields the best value for the distance-constant. For the 89 data points the distance-constant is found to be $L = 3.35$ ft. Using this value all of the data are replotted as a function of $\omega\tau_0$ as shown in Figure (16). The linear transfer function without friction is represented by the solid line in the figure. From the quality of the fit of the experimental data to the predicted linear transfer function the approximations made in arriving at Equation (43) appear reasonable.

However, there is a significant effect of the bearing friction upon the value obtained for the distance-constant. When the experimental data are reduced according to Equation (68) with $\beta_o \neq 0$, the values of $|D_1|_{exp}$ plotted in Figure (16) must be increased by an amount $(1 + \beta_o)$ which varies from point to point as β_o varies. As shown in Table 1, β_o varies from about 0.02 to about 0.09. Similarly, the theoretical expression for the transfer-function, Equation (42), which includes the effect of β_o must be used rather than Equation (43). Thus the theoretical values of $|D_1|_o$ from Equation (42) will be somewhat larger than those obtained assuming $\beta_o = 0$. The overall effect of β_o would be to shift the data in Figure (16) upward and to the right. The result is that when a least squares fit is applied to the values of $|D_1|_{exp}$ obtained from Equation (68) using Equation (42) for the expected transfer function, the distance-constant so obtained is $L = 3.52$ ft -- some 5.1 percent higher than the value obtained assuming $\beta_o = 0$. This latter value should be more realistic, and such frequency response tests in general should be analyzed so as to account for frictional effects.

No single curve such as the solid line of Figure (16) can be drawn in the case where $\beta_o \neq 0$ since the transfer function depends upon β_o as well as $\omega\tau_o$, and β_o is not constant for all of the data. However, the correlation between theoretical and experimental values of $|D_1|$ can be shown in both cases as indicated in Figures (17) and (18).

4.3 The Overspeeding Error

From Equations (40) and (64), it follows that

$$(1 + \bar{\sigma})_{exp} = \frac{K_1 \bar{E}}{K\bar{U}} (1 + \beta_o). \quad (69)$$

The experimental data obtained from the measured mean anemometer voltage according to this equation are plotted as against the values predicted from the mathematical model, Equation (38), in Figure (19). The general agreement is fair. The scatter in the data is due to two factors: 1) The sensitivity of the theoretical expression for $\bar{\sigma}$ to uncertainties in the measured values of ϵ , \bar{U} and ω , and 2) uncertainties in the measured mean voltages from both instruments. A trend is evident however, whereby the measured overspeeding error tends to be somewhat lower than the predicted values. This departure increases as the overspeeding error increases. On the average the largest overspeeding error produced in the tests was about 10 percent. The expected values were about a factor of two larger than this.

An examination of the effects of viscous friction on the propeller blades should be conducted. In general this friction will retard the rotation rate and may account for some of the average departure of the data in the figure from the expected values.

4.4 The Response Second Harmonic

From Equation (66) it follows that

$$\left| \frac{D_2}{C_2} \right|_{\text{exp}} = \frac{K_1}{K\epsilon\bar{U}} (1 + \beta_o) \left| \frac{E_2}{C_2} \right|. \quad (70)$$

The corresponding theoretical expression for the ratio of second harmonics is given by Equation (51). Instrumentation for the measurement of the phase angle ϕ_2 was not available during the course of the experiments. Consequently a direct comparison between theory and experiment is not available.

However, it can be shown that the linear transfer function is inadequate to represent the second harmonics. Figure (20) has been prepared by neglecting β_o in Equation (70). The experimental values from the resultant equation are plotted as a function of $2\omega\tau$. The solid curve represents the linear transfer function. The departure of the data from this curve is not simply experimental scatter. Departures of as much as an order of magnitude are evident. These can be qualitatively explained by the sensitivity of the second harmonic to the input fundamental amplitude, ϵ , and to the phase angle ϕ_2 as was indicated in Figures (4), (5) and (6).

Because such large departures from the linear transfer function are found experimentally, considerable doubt arises as to the adequacy of the linear transfer function for the correction of atmospheric turbulence data. This point was raised earlier in this report. Further studies are needed to quantify the spectral characteristics of helicoid anemometers.

5. CONCLUSIONS

Although perhaps heuristically, the case has been made that all rotary anemometers will exhibit the same basic dynamic response equation (as well as the same basic steady-flow response equation), and that only two experimental constants, U_o and L are required to characterize the dynamic response. Furthermore, the sinusoidal frequency response test, even with modest harmonic content present in the velocity fluctuation, provides a simple technique for determining the distance-constant. The effects of bearing friction can be accounted for as well.

The mathematical model developed accounts reasonably well for the observed overspeeding phenomenon, but probably needs refinement to account for the viscous friction on the blades of the helicoid propeller.

Sufficient doubt has been raised as to the use of a linear transfer function for the correction of measured atmospheric turbulence data to warrant further study of the effect of the inherent nonlinearities of rotary anemometers upon their spectral transfer characteristics.

The model presented can be modified to account for angles of yaw, and the basic equations derived in the text can be examined to determine

the instrument response when the mean velocity component vanishes as in the case of vertical sensors in three-component arrays.

6. ACKNOWLEDGMENTS

The authors are indebted to William G. Cleveland for his valuable assistance in performing the experiments, and to Karl E. Lofquist for his helpful discussions concerning the basic equations.

7. REFERENCES

1. G. B. Schubauer and G. H. Adams, Lag of Anemometers, NBS Report 3245, April 16, 1954.
2. P. Jepson, Currentmeter Errors Under Pulsating Flow Conditions, J. Mechanical Engineering Science 9, 1 (1967), pp. 45-54.
3. M. Rubin, R. W. Miller and W. G. Fox, Driving Torques in a Theoretical Model of a Turbine Meter, J. Basic Engineering, ASME, June 1965, pp. 413-420.
4. E. Ower, On the Response of a Vane Anemometer to An Air-Stream of Pulsating Speed, Phil. Mag. S.7. 23, 157, May 1937, pp. 992-1004.
5. J. C. Wyngaard, J. T. Bauman and R. A. Lynch, Cup Anemometer Dynamics, in FLOW, Its Measurement and Control in Science and Industry 1, Rodger B. Dowdell, Editor-in-Chief, Part 2, Flow Measuring Devices, edited by R. E. Wendt, Jr. (1972).
6. S. Ramachandran, A Theoretical Study of Cup and Vane Anemometers, Quarterly J. of the Royal Meteorological Soc. 95 (1969), pp. 163-180.
7. Rikiya Takeda, Theoretical Research on Propeller Type Current Meters, ASME Paper No. 74-WA/FM-6.
8. J. P. Bennett and R. S. McQuivey, Comparison of a Propeller Flowmeter With a Hot-Film Anemometer in Measuring Turbulence in Movable-Boundary Open-Channel Flows, U. S. Geol. Survey Prof. Paper 700-B, pp. B254-B262.
9. Thomas W. Horst, Corrections for Response Errors in a Three-Component Propeller Anemometer, J. of Applied Meteorology 12, 4, June 1973, pp. 716-725.
10. Gordon A. McBean, Instrument Requirements for Eddy Correlation Measurements, J. of Applied Meteorology 11, pp. 1078-1084.
11. B. B. Hicks, Propeller Anemometers as Sensors of Atmospheric Turbulence, Boundary-Layer Meteorology 3 (1972), pp. 214-228.

12. E. L. Deacon, The Over-Estimation Error of Cup Anemometers in Fluctuating Winds, J. of Scientific Instruments 28, August 1951, pp. 231-234.
13. Keisuke Onuma, Over-Estimation Error of Rotating Type Anemometers in Sinusoidally Fluctuating Wind Speed, Proc. 7th Japan National Congress for Applied Mechanics (1957), II-23, pp. 269-272.

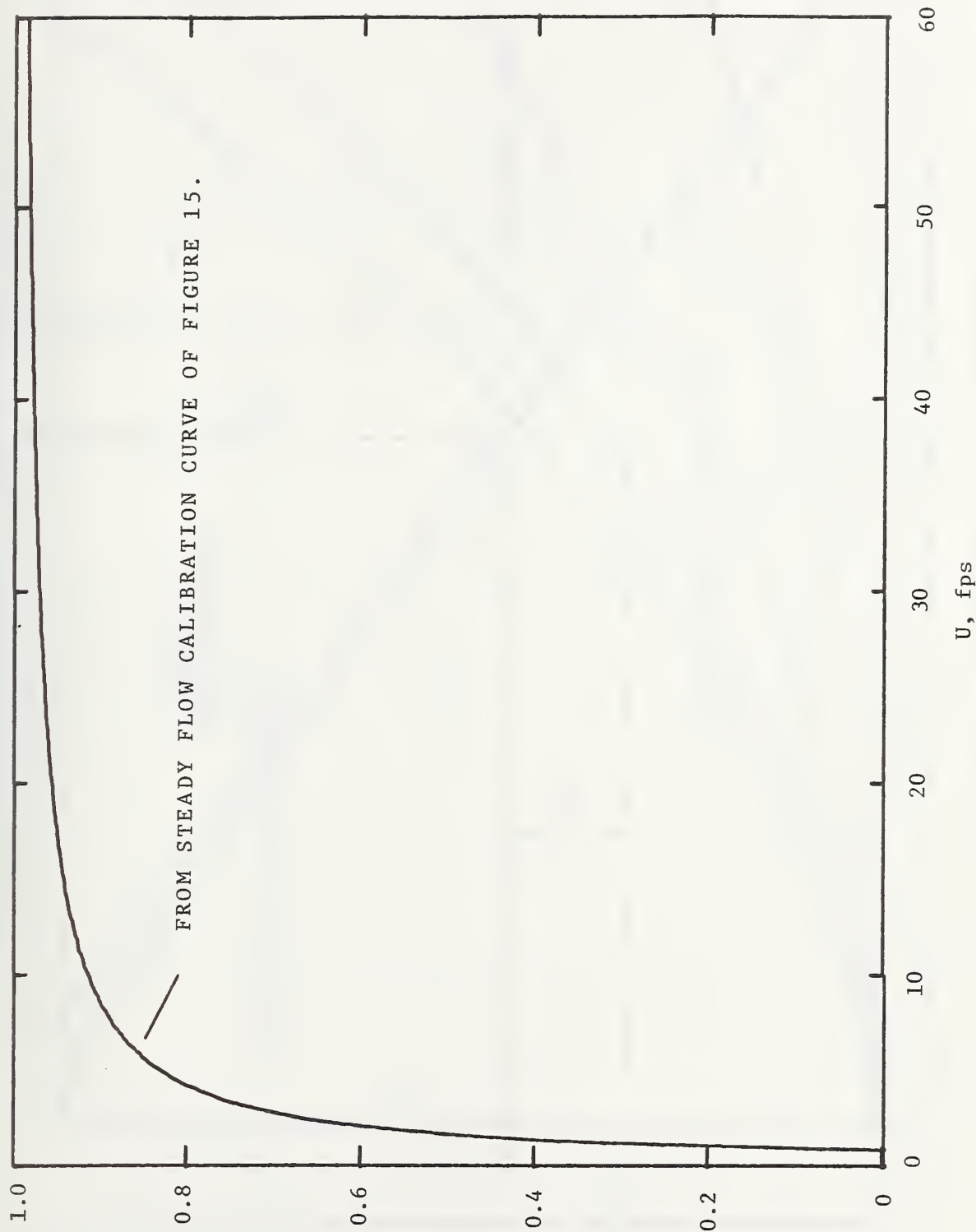


FIGURE 1. CHARACTERISTIC CURVE OF $\frac{\xi}{\xi_0}$ AS A FUNCTION OF FLOW SPEED.

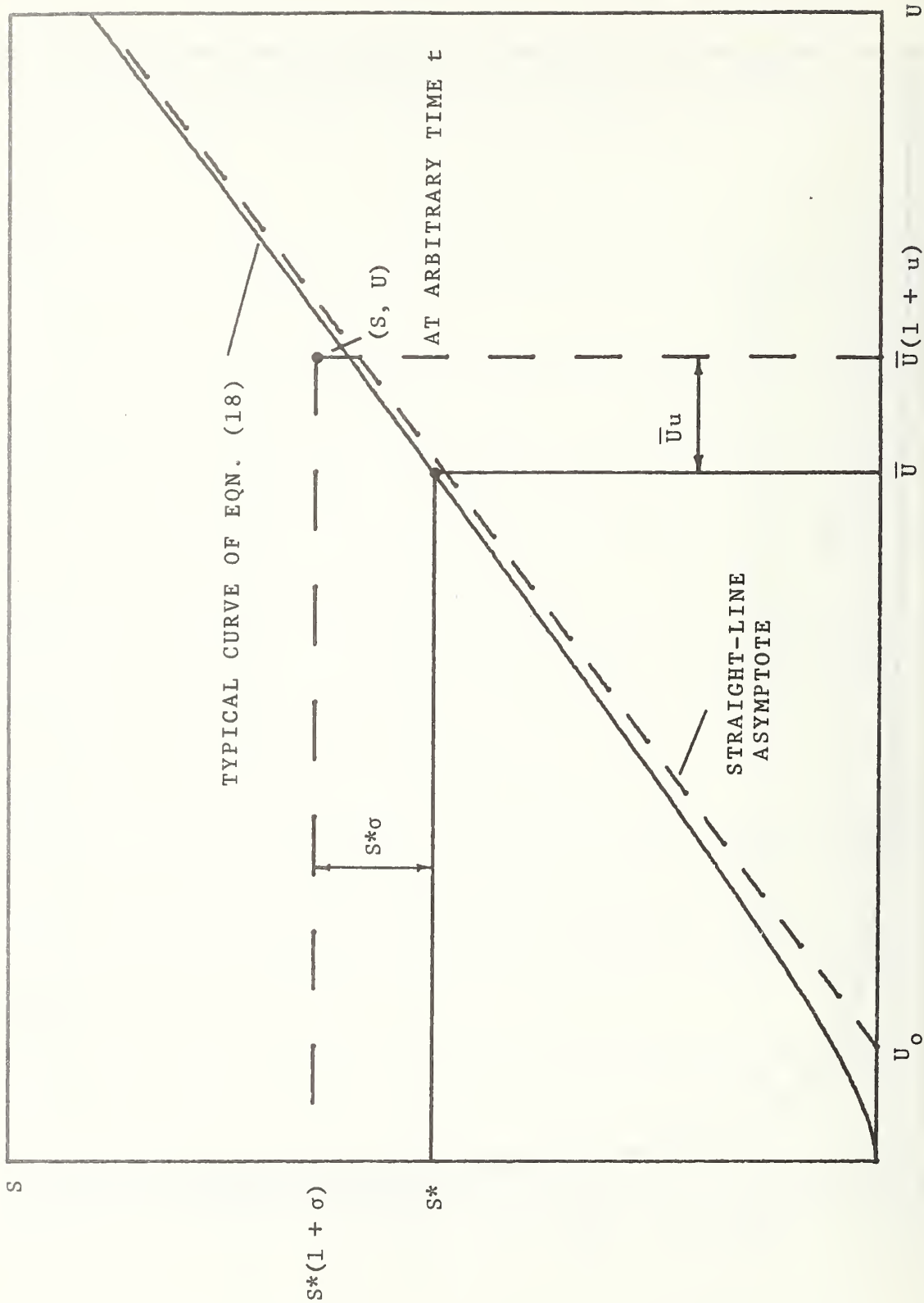


FIGURE 2. SCHEMATIC STEADY FLOW CALIBRATION CURVE DEFINING S^* AND σ .

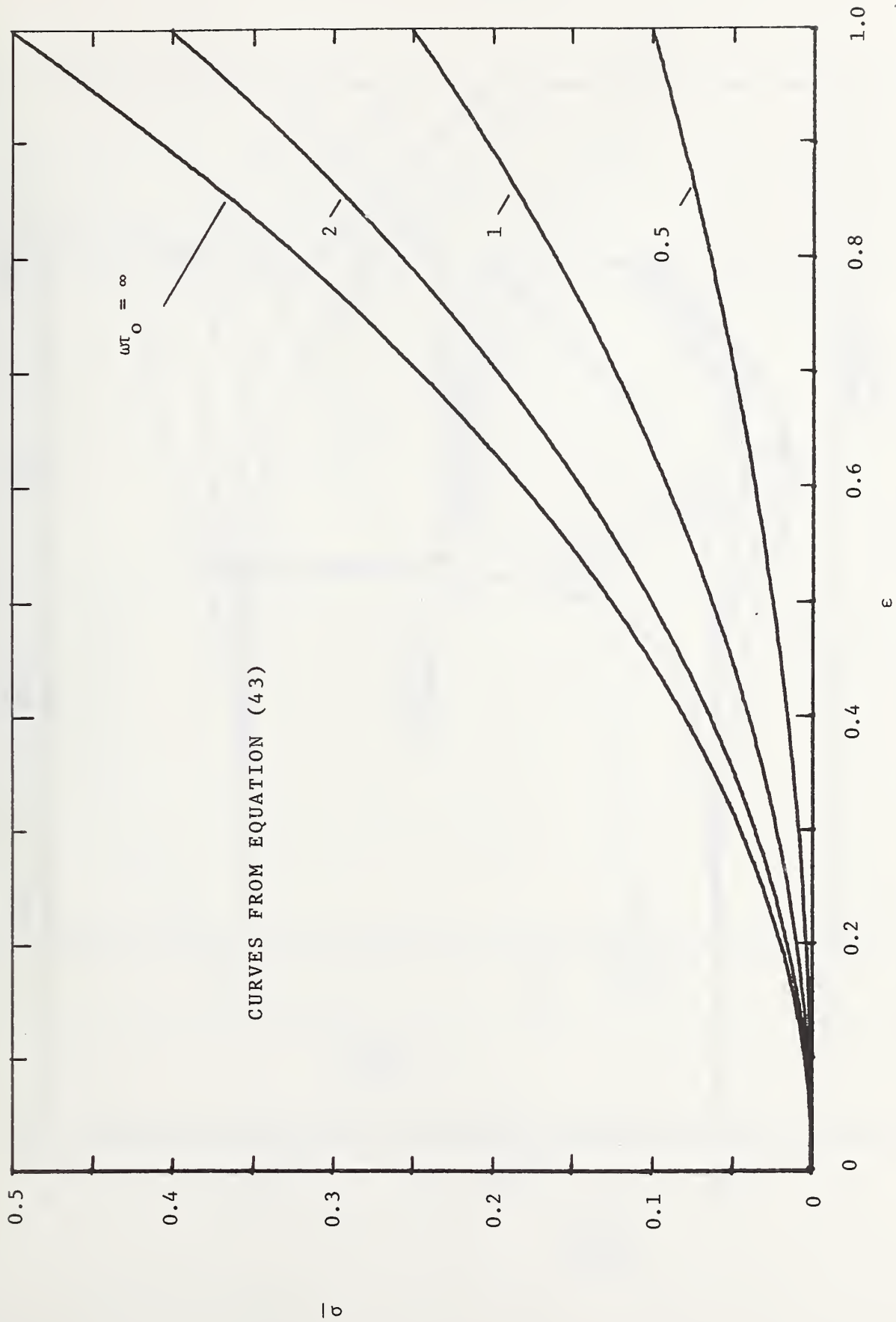


FIGURE 3. THEORETICAL OVER-REGISTRATION OF MEAN SPEED.

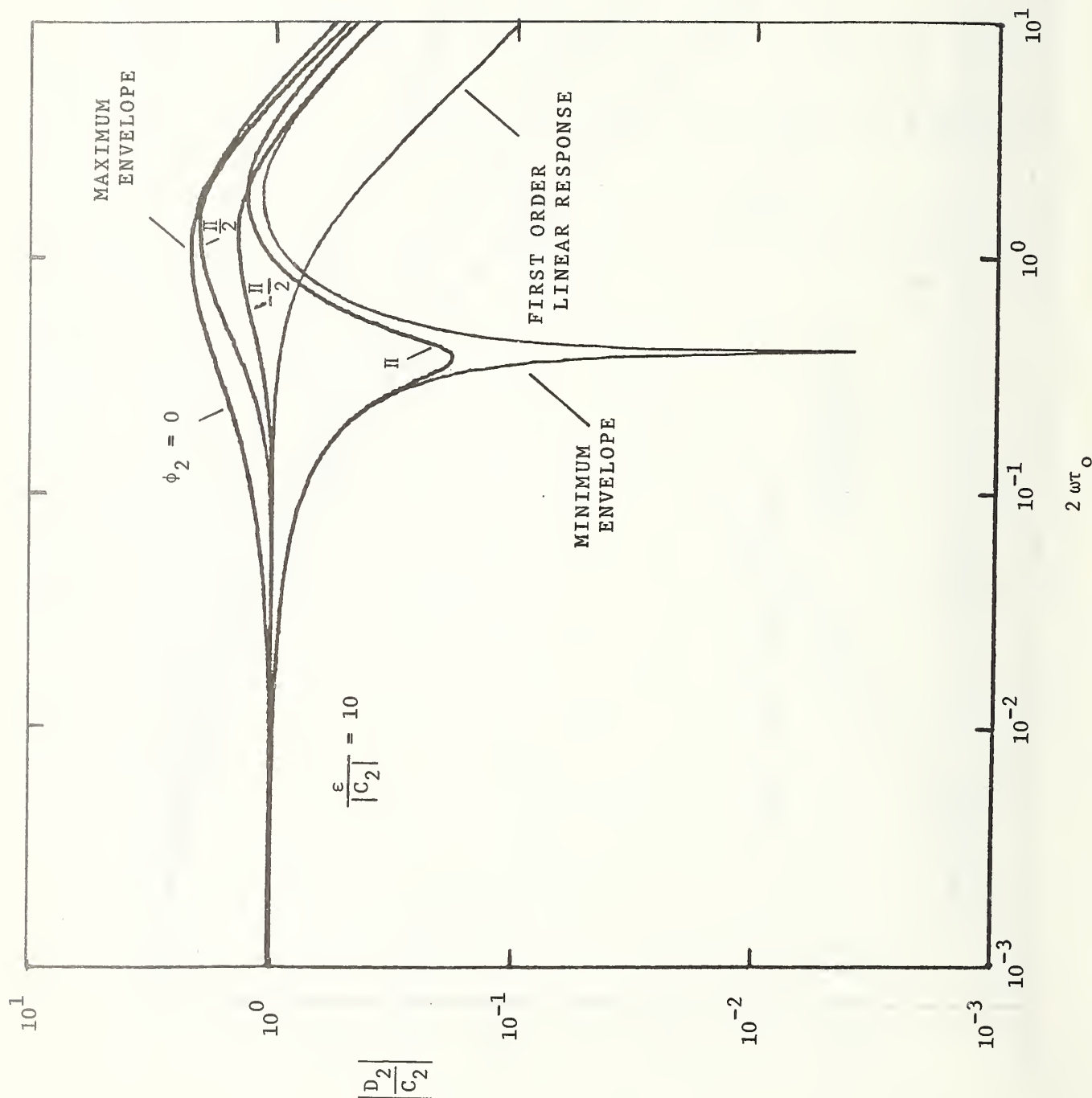


FIGURE 4. THEORETICAL PHASE DEPENDENCE OF RATIO OF SECOND HARMONICS.

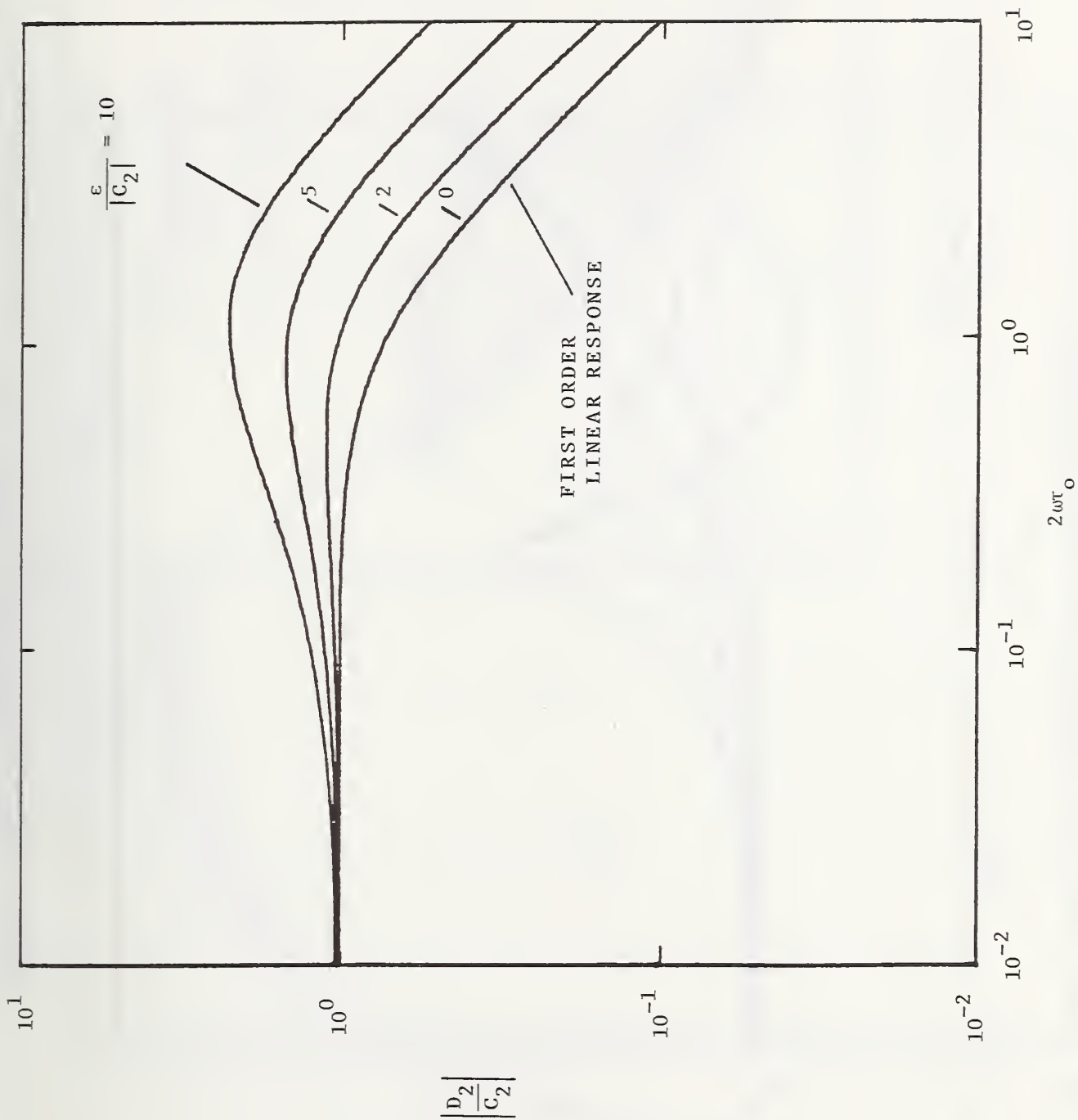


FIGURE 5. RATIO OF SECOND HARMONICS WITH $\phi_2 = 0$.

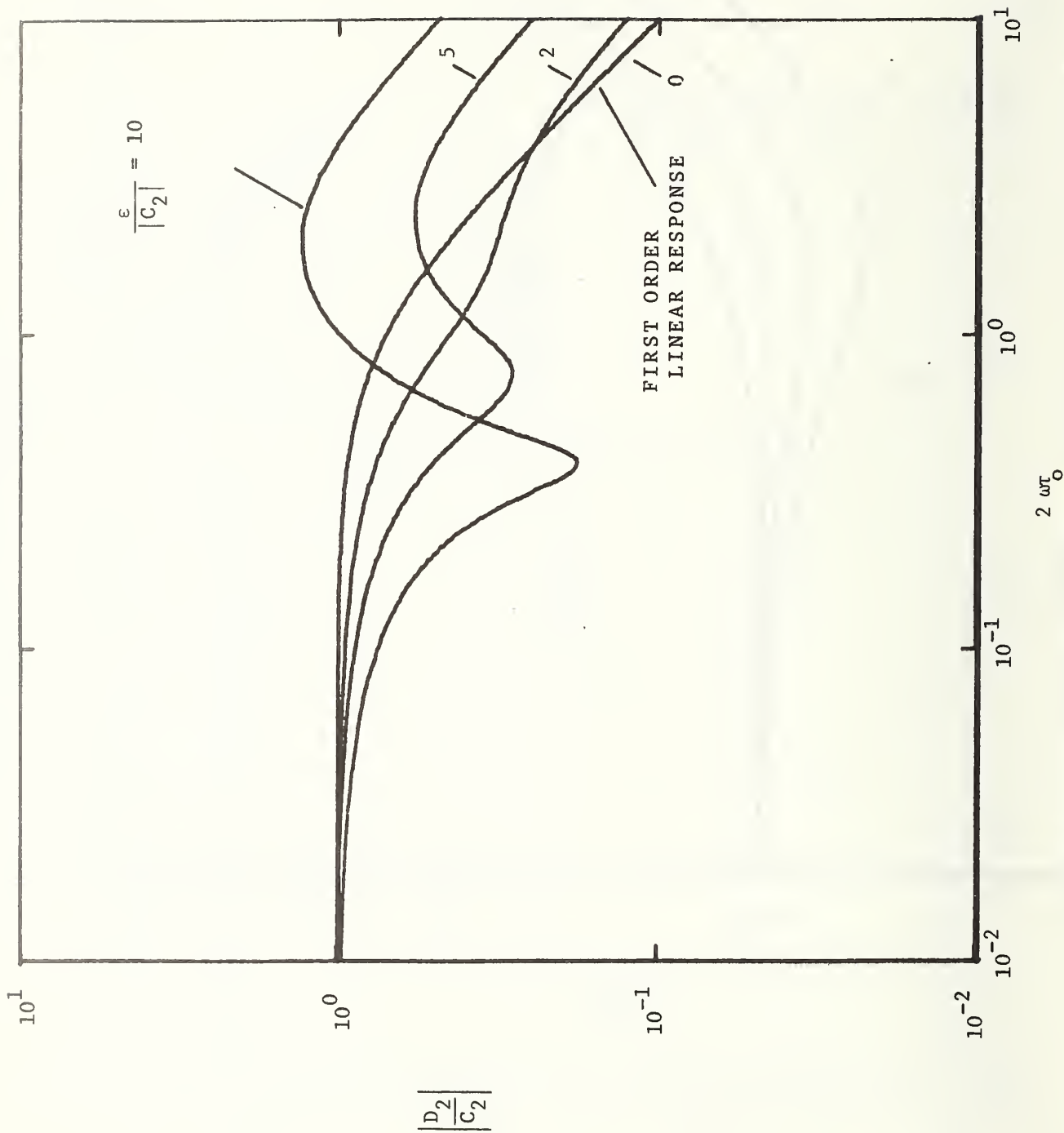


FIGURE 6. RATIO OF SECOND HARMONICS WITH $\phi_2 = \pi$.

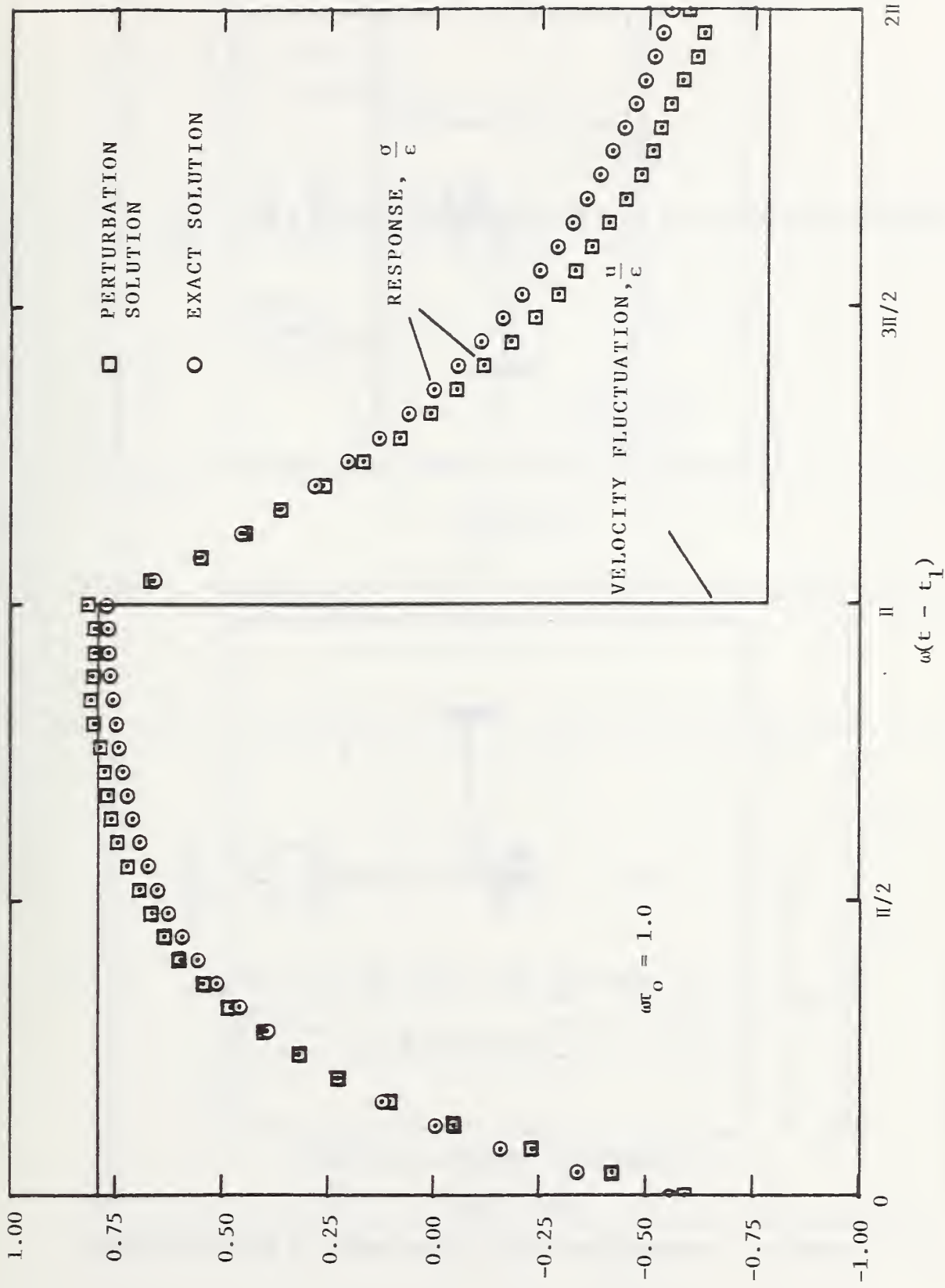
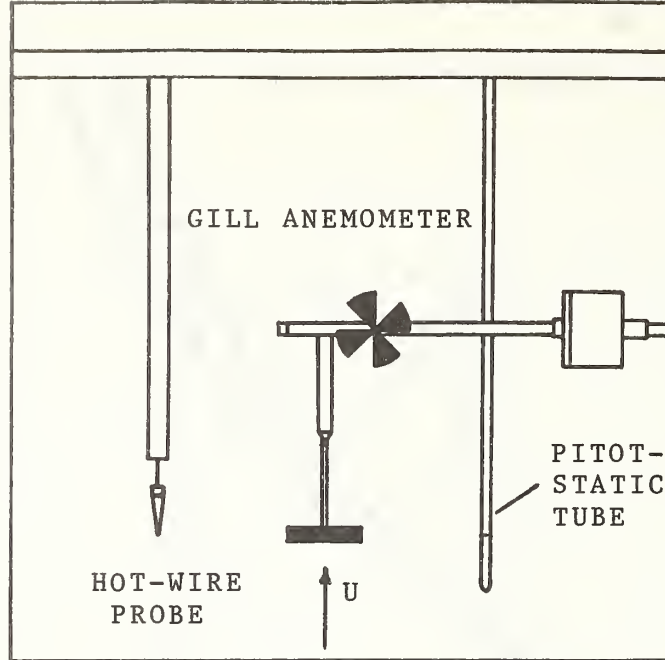
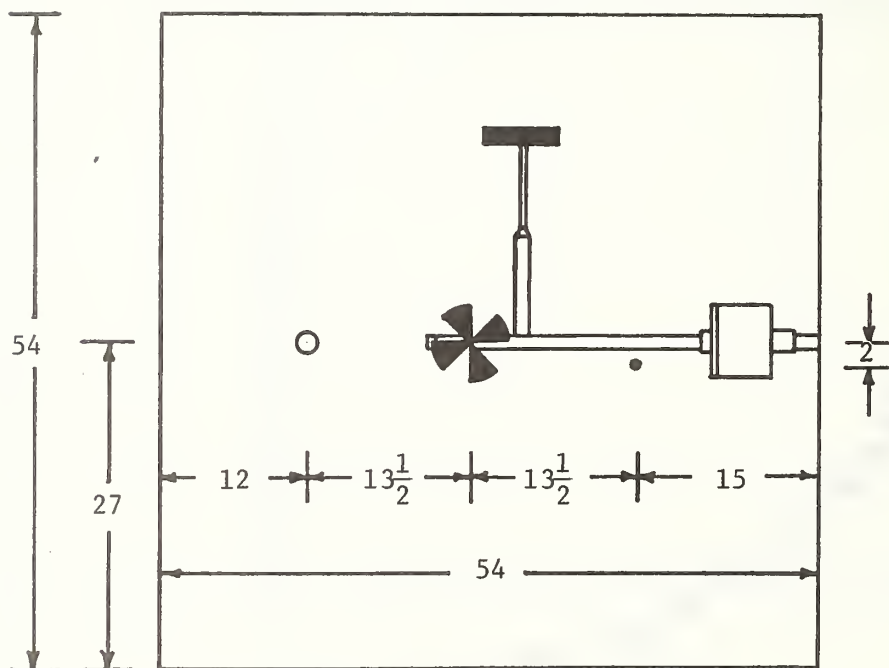


FIGURE 7. THEORETICAL, SQUARE-WAVE RESPONSE.



TOP VIEW



ALL DIMENSIONS EXPRESSED IN INCHES.

FRONT VIEW

FIGURE 8. CONFIGURATION OF THE INSTRUMENTS IN THE TEST-SECTION.

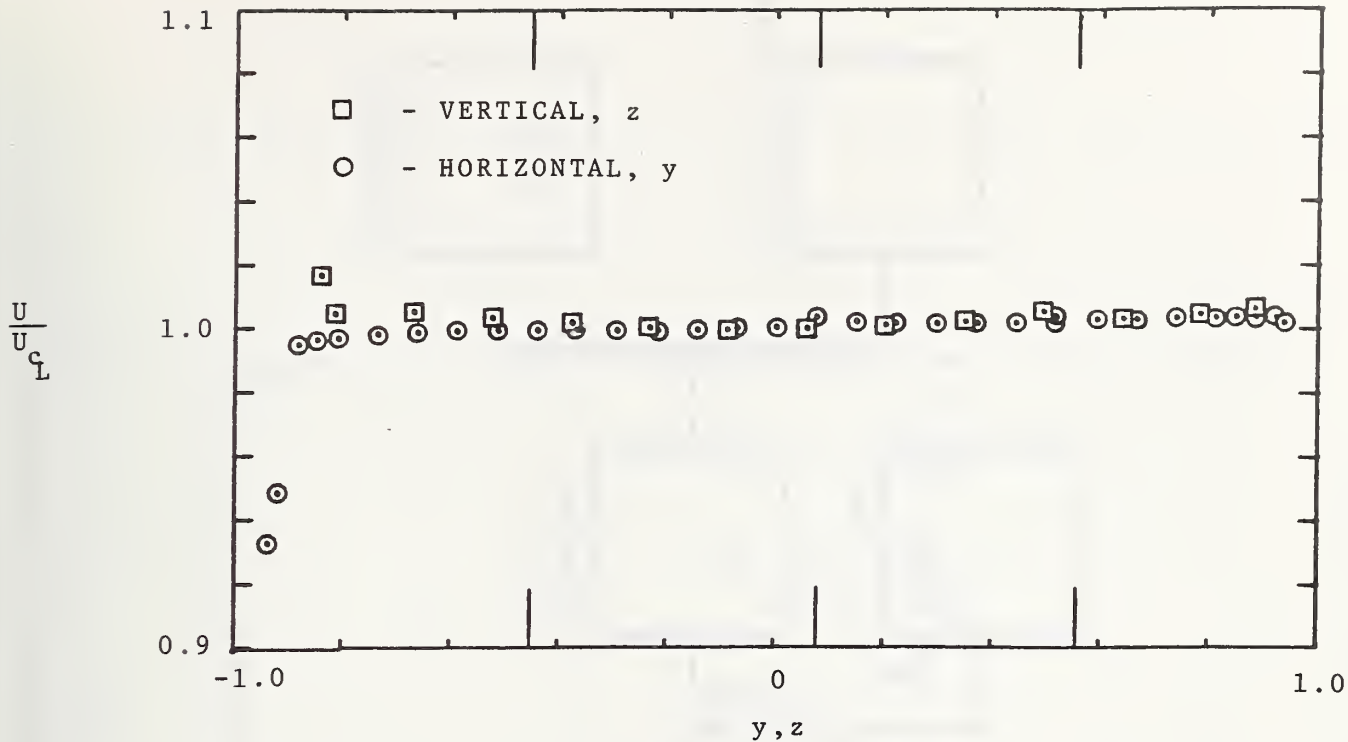


FIGURE 9. HORIZONTAL AND VERTICAL DISTRIBUTIONS OF FREE-STREAM VELOCITY, $U_{\infty} = 35$ fps

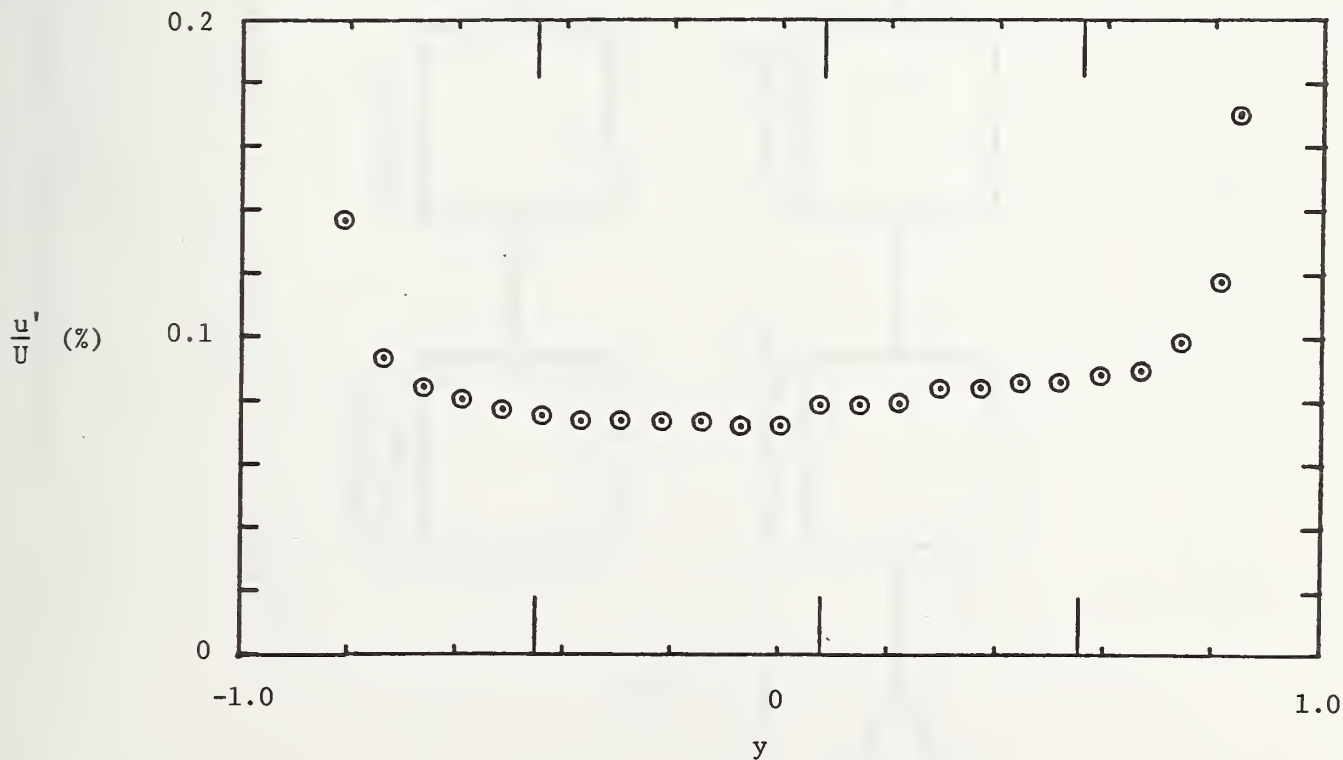


FIGURE 10. HORIZONTAL DISTRIBUTION OF FREE-STREAM LONGITUDINAL TURBULENCE INTENSITY, $U_{\infty} = 35$ fps.

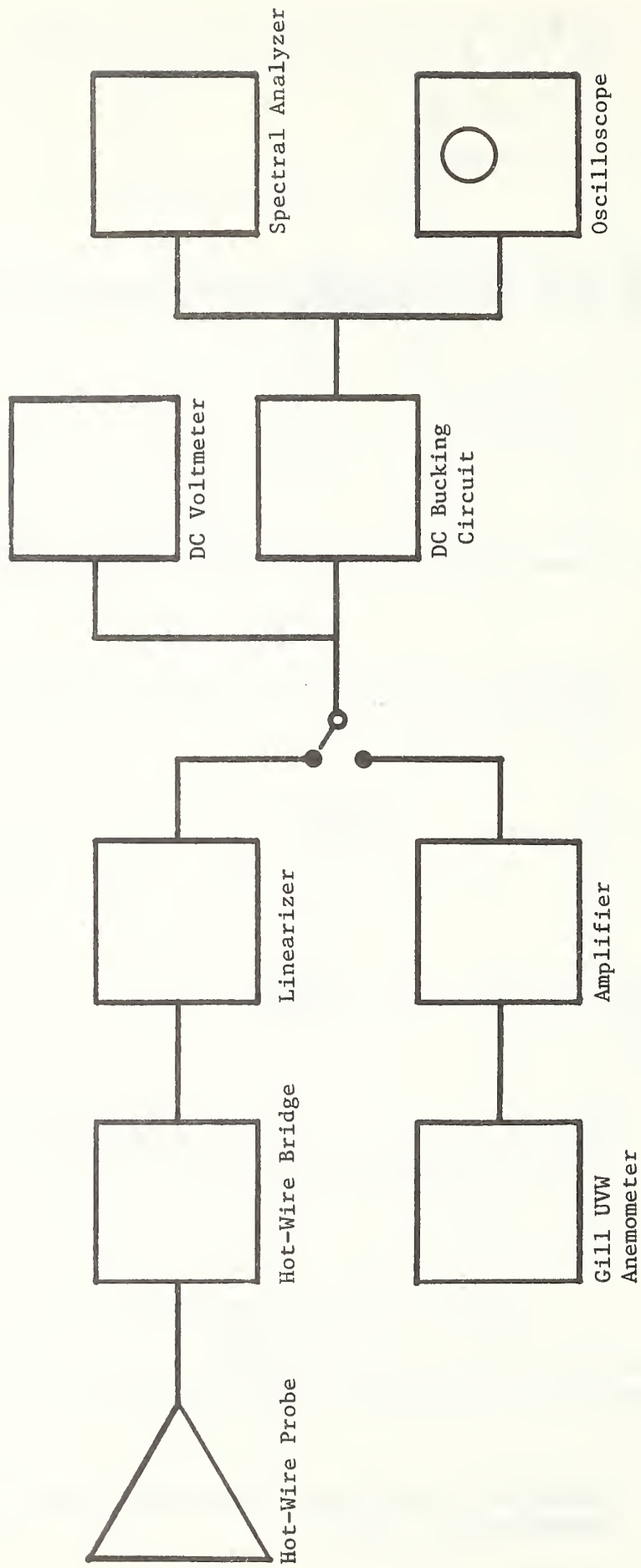


Figure 11. Instrumentation for Measured Dynamic Response Characteristics

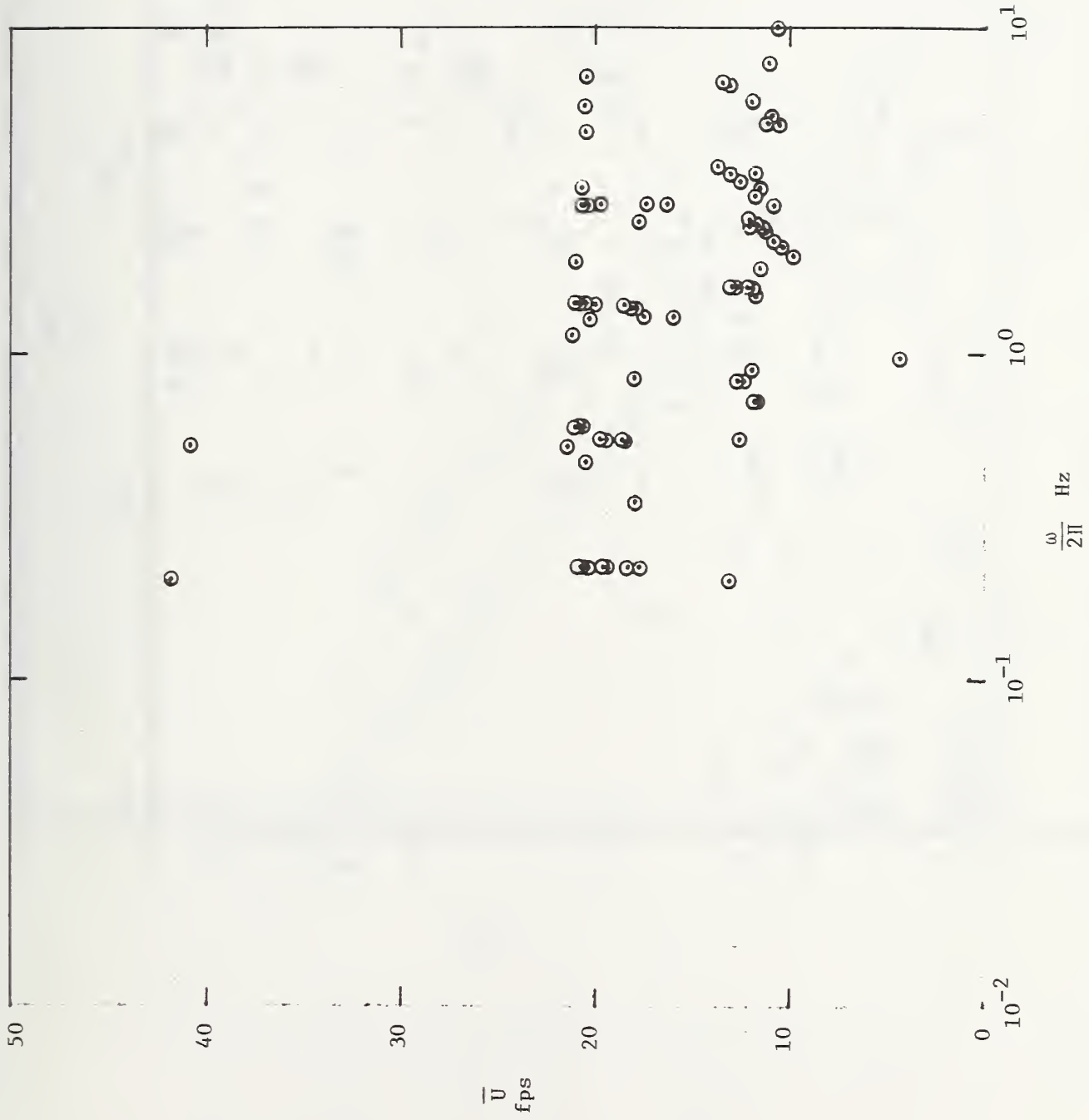


FIGURE 12. DOMAIN OF MEAN SPEED AND FREQUENCY USED IN THE EXPERIMENTS.

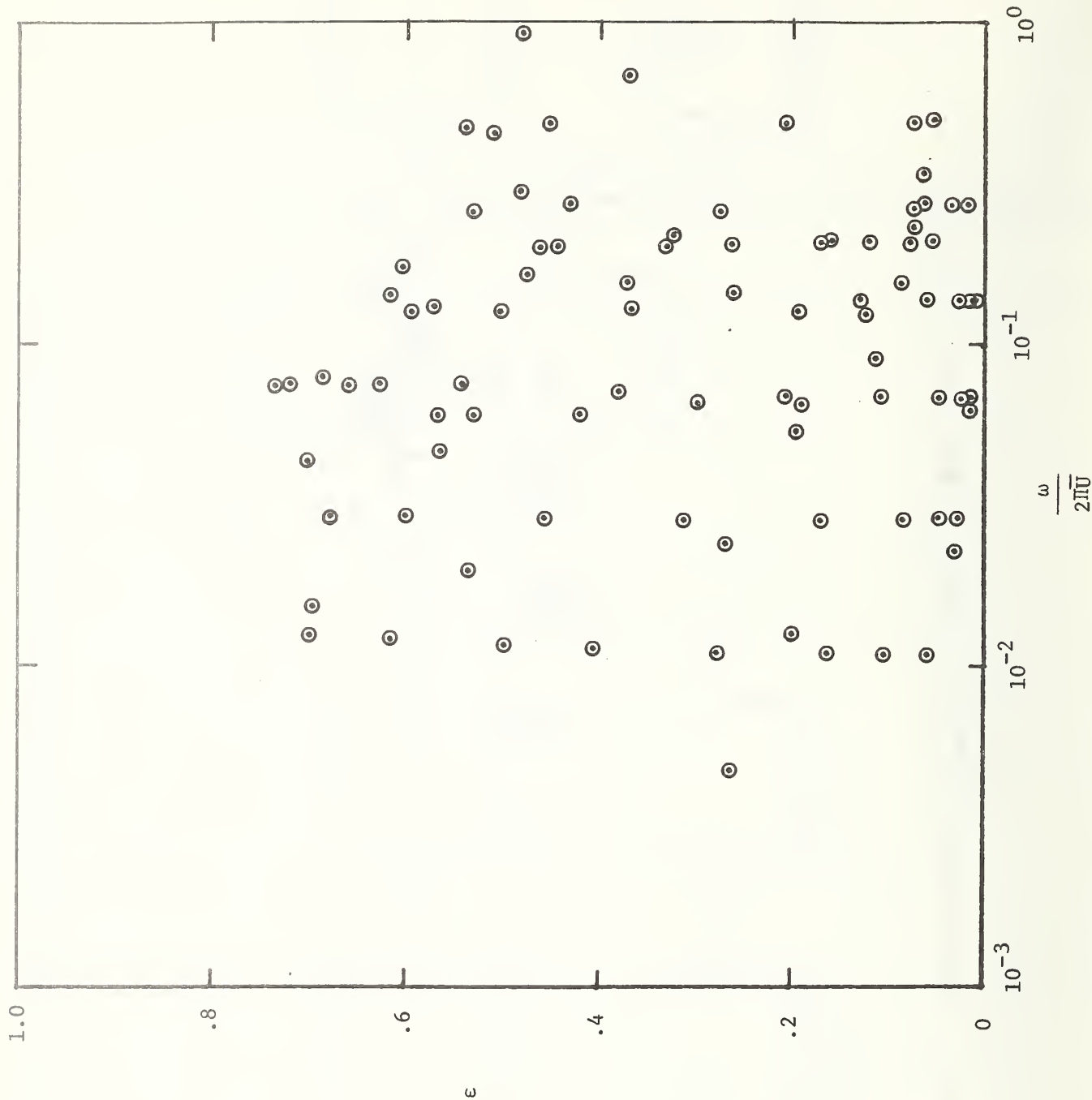


FIGURE 13. DOMAIN OF FUNDAMENTAL AMPLITUDE AND FREQUENCY COVERED BY THE EXPERIMENTS.

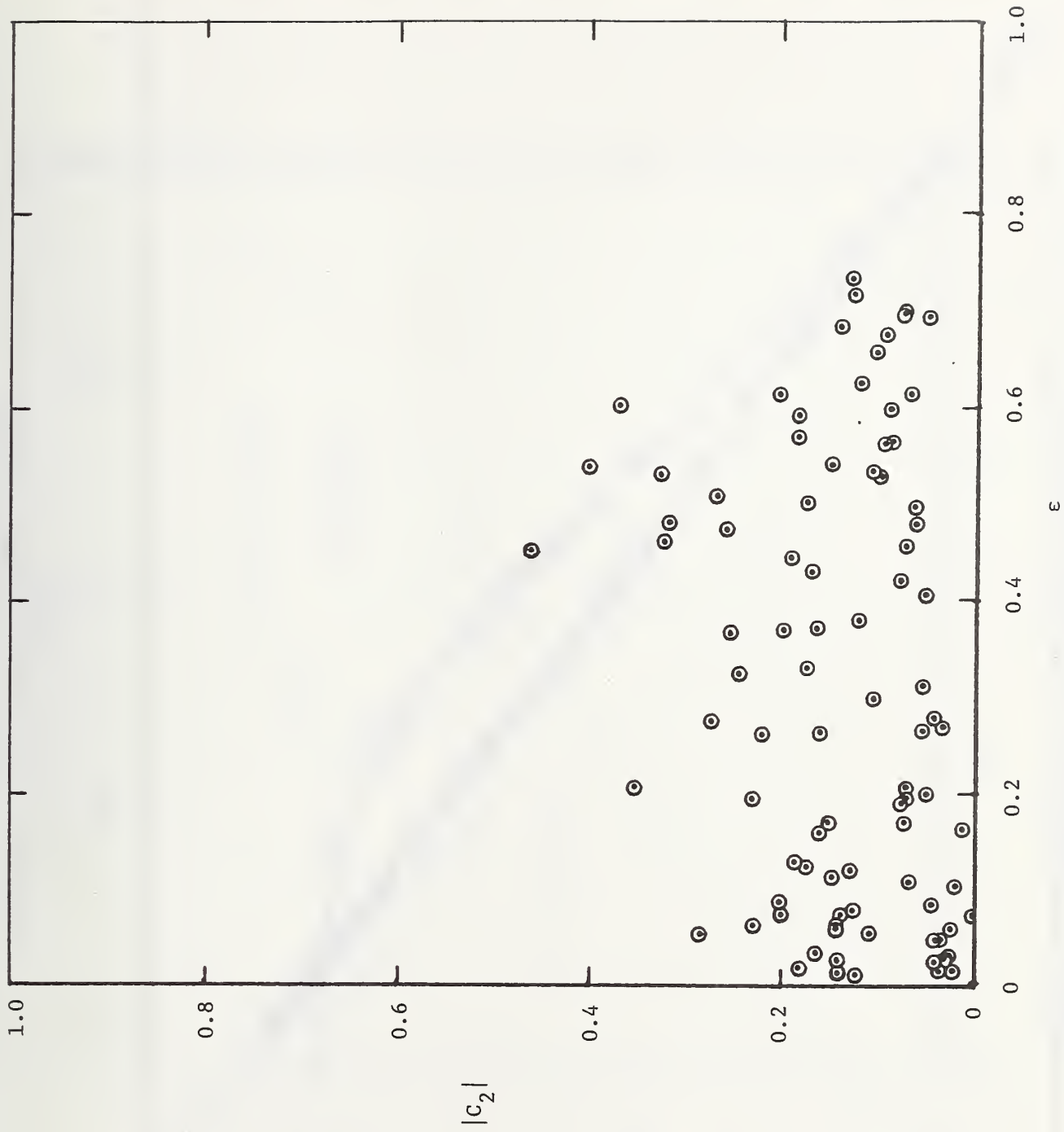


FIGURE 14. DOMAIN OF FIRST AND SECOND HARMONICS OF THE VELOCITY FLUCTUATION.

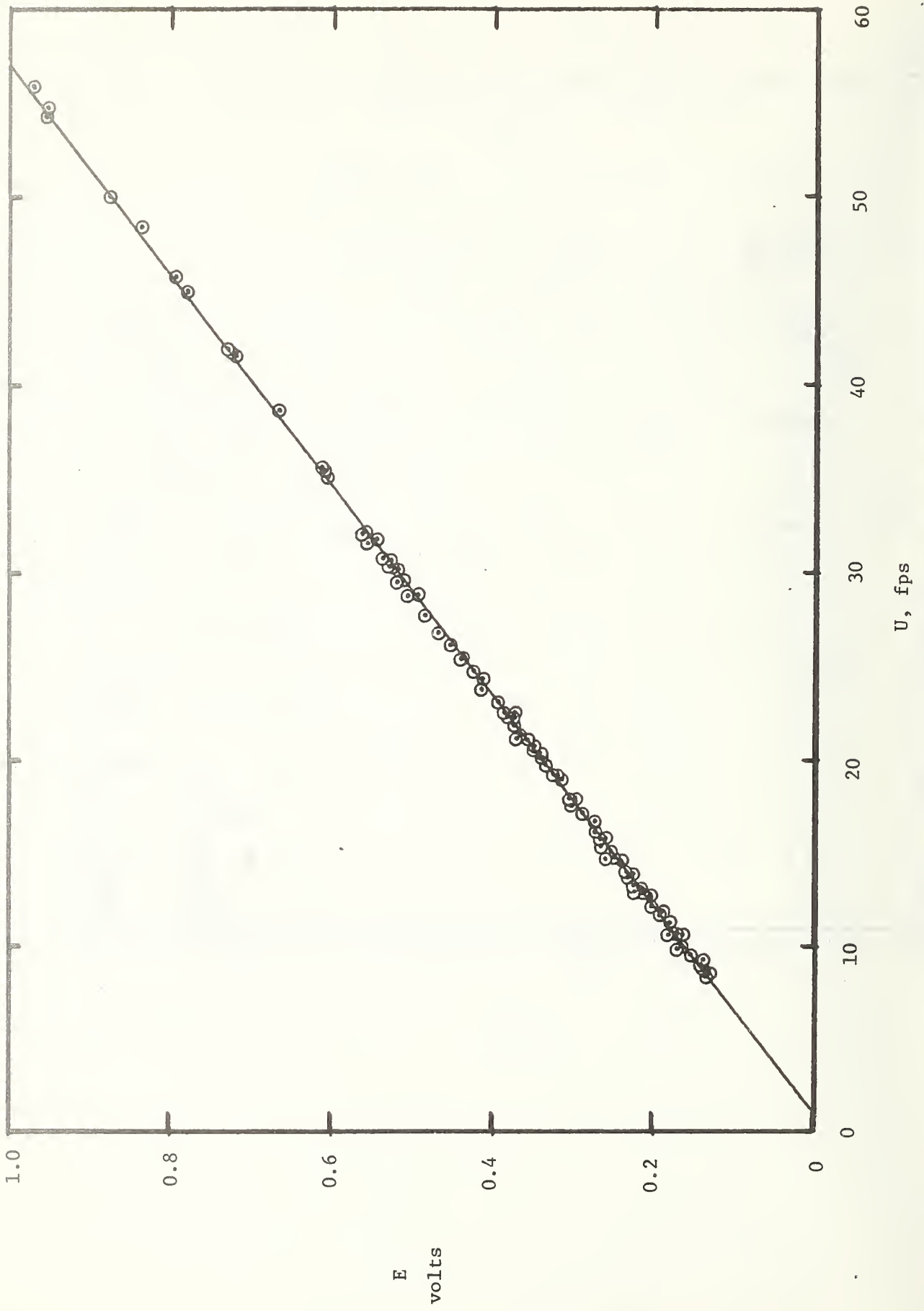


FIGURE 15. STEADY FLOW CALIBRATION CURVE.

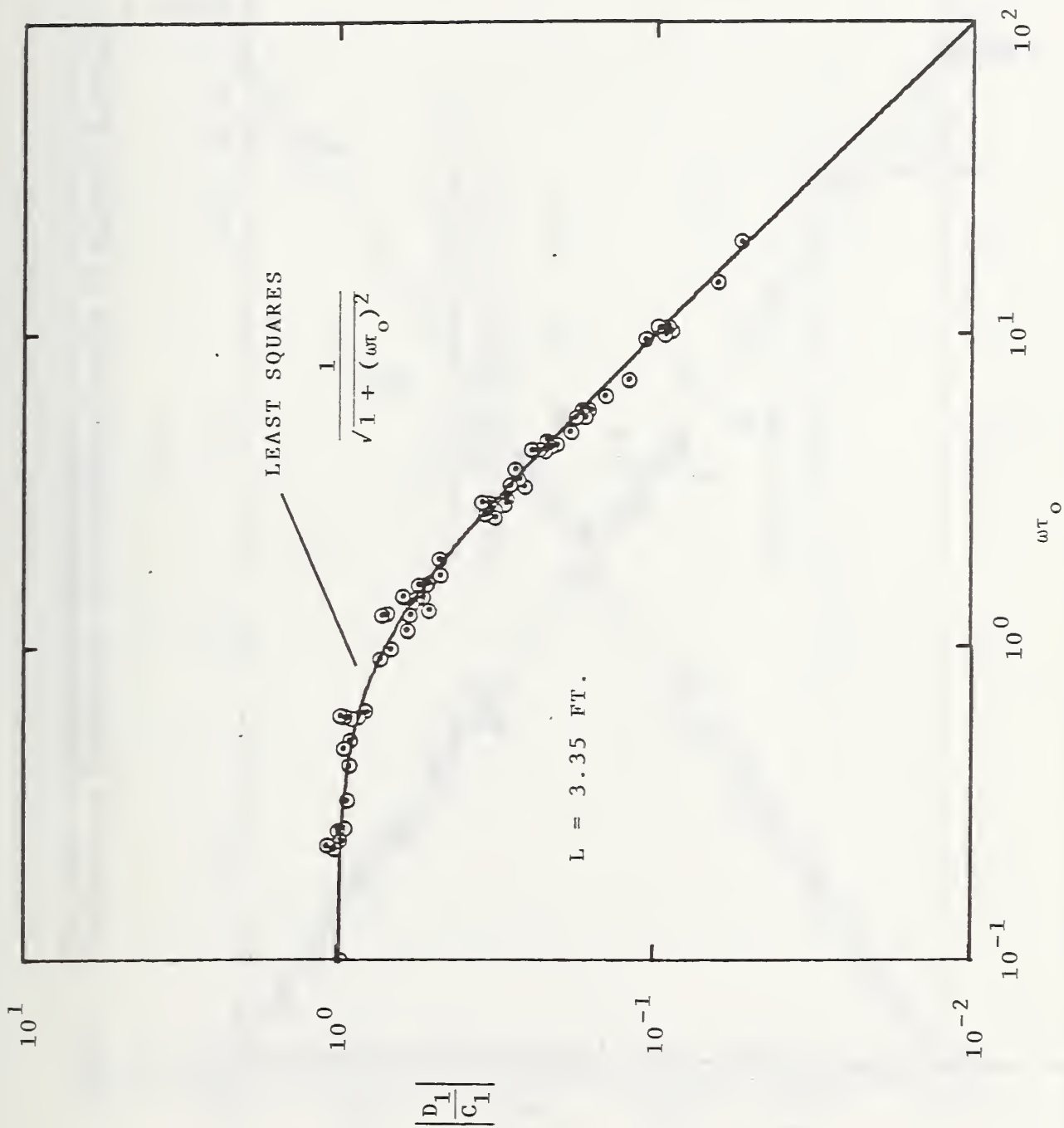


FIGURE 16. ATTENUATION OF THE RESPONSE FUNDAMENTAL.

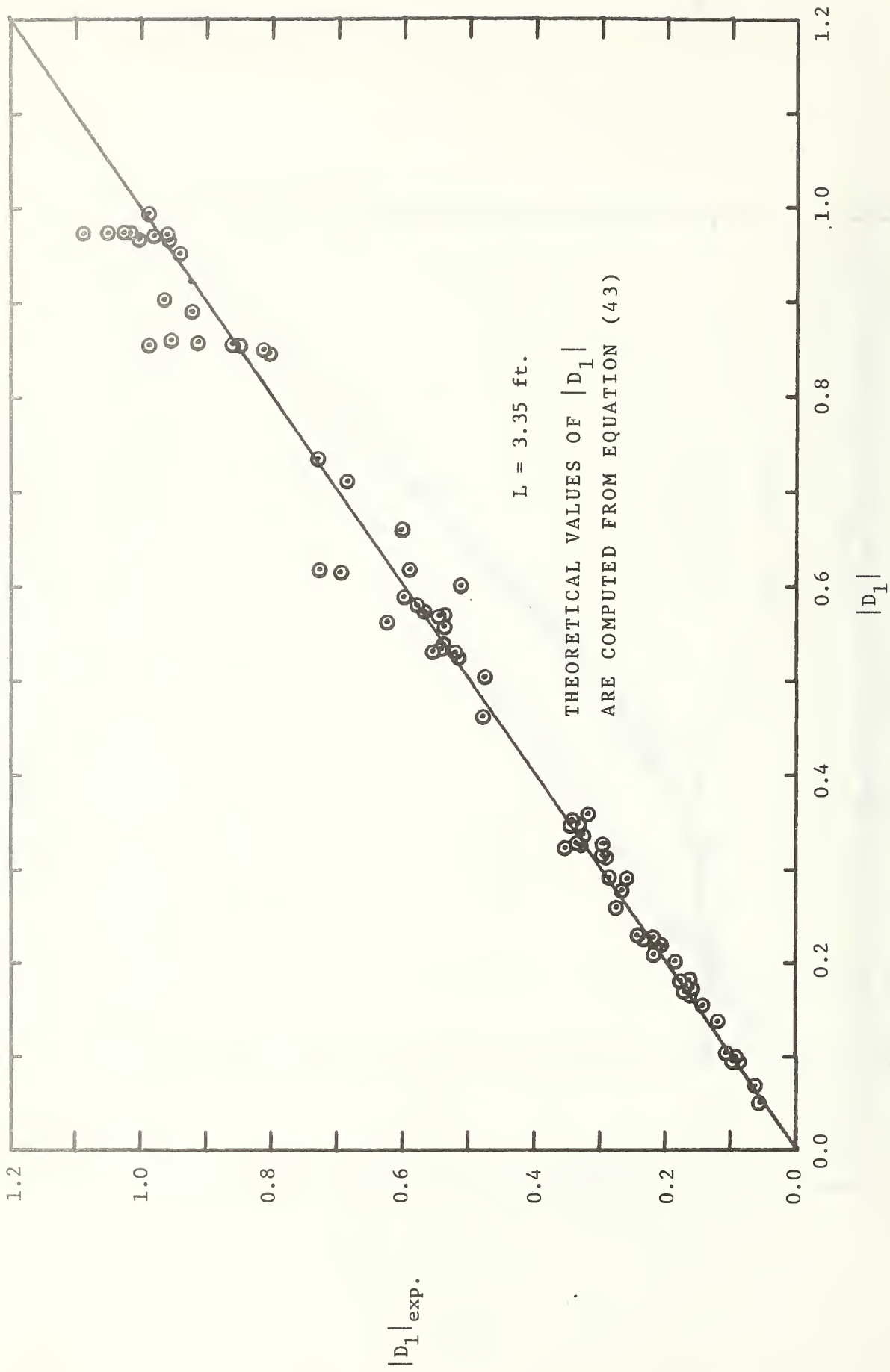


FIGURE 17. COMPARISON OF THEORETICAL AND EXPERIMENTAL VALUES OF RESPONSE FUNDAMENTAL AMPLITUDE, NEGLECTING BEARING FRICTION.

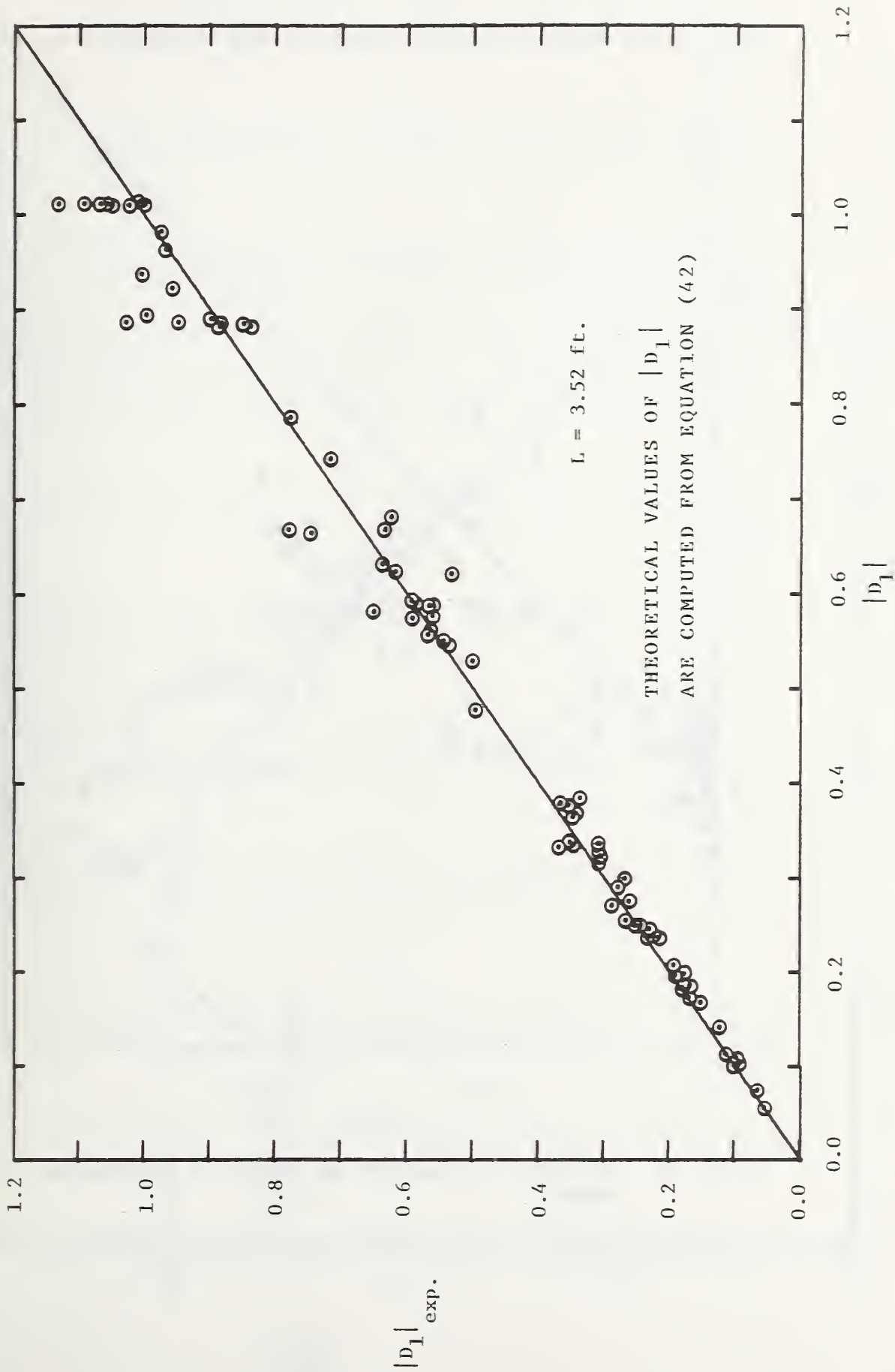


FIGURE 18. COMPARISON OF THEORETICAL AND EXPERIMENTAL VALUES OF RESPONSE FUNDAMENTAL AMPLITUDE, WITH BEARING FRICTION.

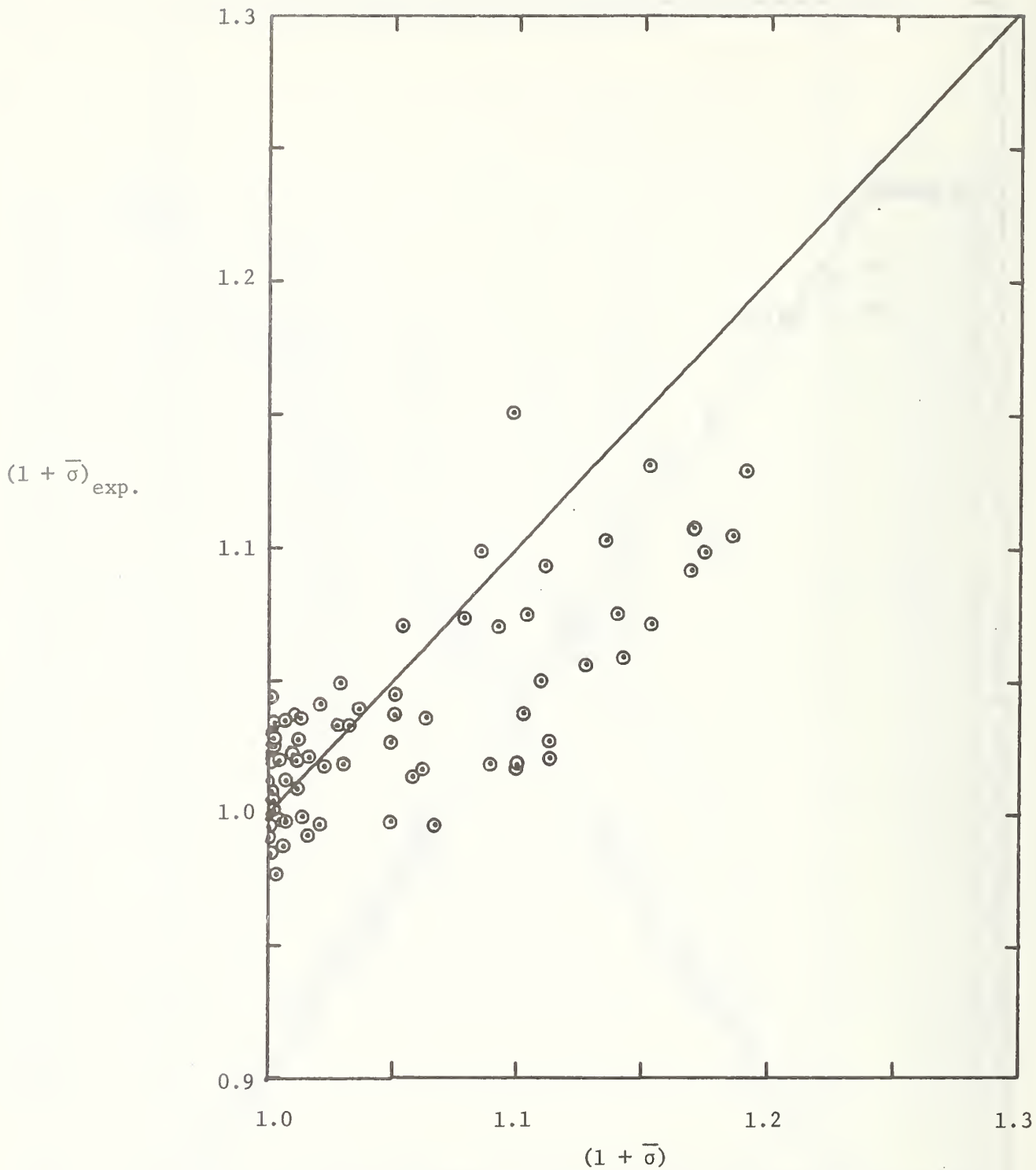


FIGURE 19. COMPARISON OF MEASURED AND PREDICTED OVERSPEEDING ERRORS.

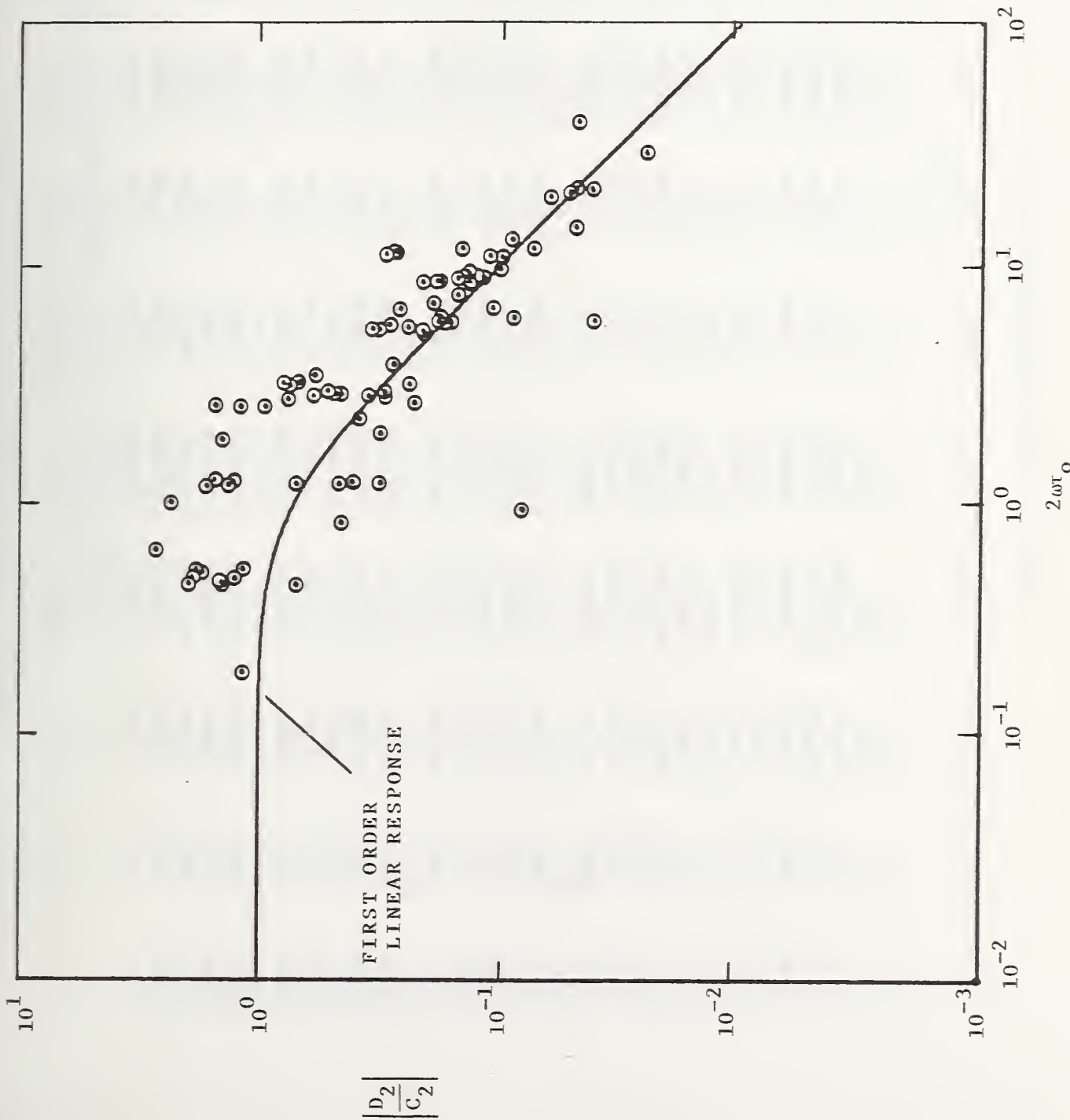


FIGURE 20. RESPONSE OF SECOND HARMONIC.

Table 1. Table of Experimental Data

| $\frac{\omega}{2\pi}$ | \bar{U} | ϵ | $\epsilon C_2 $ | β_0 | $ D_1 $ | $ D_1 $ ($\beta_0 \neq 0$) | $ D_2 $ | $ D_2 $ ($\beta_0 \neq 0$) | $1 + \bar{\sigma}$ | $1 + \bar{\sigma}$ ($\beta_0 \neq 0$) |
|-----------------------|-----------|------------|-----------------|-----------|---------|---------------------------------|---------|---------------------------------|--------------------|--------------------------------------------|
| 0.52 | 21.4 | 0.269 | 0.0093 | 0.0397 | 0.92 | 0.96 | 0.081 | 0.084 | 1.00 | 1.00 |
| 1.14 | 21.1 | 0.194 | 0.0139 | 0.0404 | 0.60 | 0.63 | 0.028 | 0.029 | 1.02 | 1.02 |
| 1.90 | 20.9 | 0.111 | 0.0164 | 0.0407 | 0.48 | 0.50 | 0.042 | 0.044 | 1.02 | 1.02 |
| 3.22 | 20.6 | 0.084 | 0.0170 | 0.0413 | 0.26 | 0.27 | 0.022 | 0.023 | 1.03 | 1.03 |
| 5.70 | 20.5 | 0.060 | 0.0138 | 0.0415 | 0.16 | 0.17 | 0.017 | 0.018 | 1.02 | 1.02 |
| 7.00 | 20.4 | 0.063 | 0.0089 | 0.0416 | 0.12 | 0.12 | 0.007 | 0.007 | 1.03 | 1.03 |
| 4.72 | 20.5 | 0.073 | 0.0100 | 0.0415 | 0.19 | 0.20 | 0.014 | 0.015 | 1.03 | 1.03 |
| 0.46 | 20.4 | 0.029 | 0.0007 | 0.0417 | 0.96 | 1.01 | 0.002 | 0.002 | 1.02 | 1.02 |
| 1.28 | 20.2 | 0.013 | 0.0003 | 0.0421 | 0.51 | 0.53 | 0.005 | 0.005 | 1.03 | 1.03 |
| 0.22 | 20.7 | 0.059 | 0.0015 | 0.0412 | 1.03 | 1.07 | 0.018 | 0.019 | 0.99 | 0.99 |
| 0.22 | 20.6 | 0.104 | 0.0020 | 0.0413 | 1.05 | 1.09 | 0.027 | 0.028 | 1.00 | 1.00 |
| 0.22 | 20.4 | 0.162 | 0.0019 | 0.0418 | 1.02 | 1.06 | 0.023 | 0.024 | 1.00 | 1.00 |
| 0.22 | 20.2 | 0.278 | 0.0121 | 0.0422 | 1.09 | 1.13 | 0.063 | 0.066 | 1.01 | 1.01 |
| 0.22 | 19.5 | 0.405 | 0.0218 | 0.0435 | 0.96 | 1.00 | 0.068 | 0.071 | 1.00 | 1.00 |
| 0.22 | 19.2 | 0.497 | 0.0321 | 0.0444 | 0.98 | 1.02 | 0.122 | 0.127 | 1.01 | 1.01 |
| 0.22 | 18.2 | 0.614 | 0.0424 | 0.0467 | 1.00 | 1.05 | 0.120 | 0.126 | 1.01 | 1.01 |
| 0.22 | 17.6 | 0.698 | 0.0535 | 0.0484 | 1.00 | 1.05 | 0.141 | 0.148 | 1.02 | 1.02 |
| 0.54 | 18.5 | 0.674 | 0.0636 | 0.0460 | 0.81 | 0.85 | 0.123 | 0.129 | 1.04 | 1.04 |
| 0.56 | 18.6 | 0.597 | 0.0526 | 0.0457 | 0.80 | 0.84 | 0.136 | 0.142 | 1.04 | 1.04 |
| 0.56 | 19.4 | 0.454 | 0.0321 | 0.0438 | 0.86 | 0.90 | 0.096 | 0.100 | 1.03 | 1.03 |
| 0.56 | 19.7 | 0.310 | 0.0167 | 0.0432 | 0.96 | 1.00 | 0.089 | 0.093 | 1.03 | 1.03 |
| 0.60 | 21.0 | 0.167 | 0.0123 | 0.0406 | 0.91 | 0.95 | 0.052 | 0.054 | 0.98 | 0.98 |
| 0.60 | 20.7 | 0.082 | 0.0036 | 0.0411 | 0.85 | 0.89 | 0.014 | 0.015 | 1.00 | 1.00 |
| 0.60 | 20.5 | 0.046 | 0.0015 | 0.0414 | 0.85 | 0.89 | 0.014 | 0.015 | 1.01 | 1.01 |
| 0.60 | 20.9 | 0.025 | 0.0007 | 0.0408 | 0.99 | 1.03 | 0.014 | 0.015 | 1.02 | 1.02 |

Table 1. Table of Experimental Data (Continued)

| $\frac{\omega}{2\pi}$ | \bar{U} | ϵ | $\epsilon C_2 $ | β_0 | $ D_1 $ | $ D_1 $ ($\beta_0 \neq 0$) | $ D_2 $ | $ D_2 $ ($\beta_0 \neq 0$) | $1 + \bar{\sigma}$ | $1 + \bar{\sigma}$ ($\beta_0 \neq 0$) |
|-----------------------|-----------|------------|-----------------|-----------|---------|---------------------------------|---------|---------------------------------|--------------------|--------------------------------------------|
| 7.70 | 11.1 | 0.367 | 0.0724 | 0.0766 | 0.06 | 0.07 | 0.005 | 0.005 | 1.00 | 1.00 |
| 0.20 | 41.8 | 0.263 | 0.0139 | 0.0204 | 0.99 | 1.01 | 0.063 | 0.064 | 0.99 | 0.99 |
| 0.52 | 40.7 | 0.197 | 0.0097 | 0.0209 | 0.96 | 0.97 | 0.058 | 0.059 | 1.01 | 1.01 |
| 1.50 | 11.8 | 0.592 | 0.1089 | 0.0723 | 0.34 | 0.37 | 0.064 | 0.069 | 1.07 | 1.07 |
| 1.50 | 11.7 | 0.500 | 0.0868 | 0.0726 | 0.33 | 0.36 | 0.056 | 0.060 | 1.05 | 1.05 |
| 1.60 | 12.2 | 0.364 | 0.0924 | 0.0697 | 0.32 | 0.35 | 0.062 | 0.066 | 1.02 | 1.01 |
| 1.60 | 12.7 | 0.192 | 0.0439 | 0.0668 | 0.34 | 0.37 | 0.049 | 0.052 | 1.00 | 0.99 |
| 1.60 | 13.0 | 0.122 | 0.0209 | 0.0656 | 0.32 | 0.34 | 0.036 | 0.038 | 0.99 | 0.99 |
| 0.82 | 12.6 | 0.190 | 0.0140 | 0.0676 | 0.60 | 0.64 | 0.057 | 0.061 | 1.04 | 1.04 |
| 0.82 | 12.3 | 0.298 | 0.0316 | 0.0694 | 0.58 | 0.62 | 0.064 | 0.068 | 1.05 | 1.05 |
| 0.71 | 11.7 | 0.420 | 0.0322 | 0.0725 | 0.59 | 0.63 | 0.073 | 0.078 | 1.07 | 1.07 |
| 0.71 | 11.7 | 0.528 | 0.0522 | 0.0725 | 0.73 | 0.78 | 0.119 | 0.128 | 1.10 | 1.10 |
| 0.71 | 11.6 | 0.566 | 0.0486 | 0.0732 | 0.70 | 0.75 | 0.132 | 0.142 | 1.14 | 1.15 |
| 5.00 | 10.5 | 0.536 | 0.2158 | 0.0807 | 0.09 | 0.10 | 0.021 | 0.023 | 1.06 | 1.06 |
| 5.90 | 12.0 | 0.205 | 0.0718 | 0.0706 | 0.09 | 0.10 | 0.015 | 0.016 | 1.00 | 1.00 |
| 6.60 | 13.1 | 0.051 | 0.0144 | 0.0649 | 0.09 | 0.10 | 0.000 | 0.000 | 0.99 | 0.99 |
| 3.00 | 11.7 | 0.274 | 0.0747 | 0.0727 | 0.17 | 0.18 | 0.027 | 0.029 | 1.04 | 1.04 |
| 2.80 | 10.8 | 0.530 | 0.1734 | 0.0788 | 0.18 | 0.19 | 0.037 | 0.040 | 1.10 | 1.10 |
| 6.70 | 13.5 | 0.071 | 0.0000 | 0.0631 | 0.10 | 0.10 | 0.001 | 0.001 | 1.00 | 1.00 |
| 3.70 | 13.7 | 0.016 | 0.0028 | 0.0622 | 0.16 | 0.17 | 0.051 | 0.054 | 1.02 | 1.02 |
| 3.50 | 13.0 | 0.034 | 0.0055 | 0.0652 | 0.16 | 0.17 | 0.044 | 0.047 | 1.02 | 1.02 |
| 3.30 | 12.5 | 0.074 | 0.0147 | 0.0678 | 0.17 | 0.18 | 0.061 | 0.065 | 1.01 | 1.01 |
| 1.97 | 9.8 | 0.442 | 0.0842 | 0.0866 | 0.25 | 0.27 | 0.041 | 0.045 | 1.07 | 1.07 |
| 2.12 | 10.4 | 0.328 | 0.0562 | 0.0818 | 0.24 | 0.26 | 0.032 | 0.035 | 1.05 | 1.05 |
| 2.43 | 11.4 | 0.156 | 0.0248 | 0.0744 | 0.20 | 0.22 | 0.023 | 0.025 | 1.02 | 1.02 |

Table 1. Table of Experimental Data (Continued)

| $\frac{\omega}{2\pi}$ | \bar{U} | ϵ | $\epsilon C_2 $ | β_0 | $ D_1 $ | $ D_1 $ ($\beta_0 \neq 0$) | $ D_2 $ | $ D_2 $ ($\beta_0 \neq 0$) | $1 + \bar{\sigma}$ | $1 + \bar{\sigma}$ ($\beta_0 \neq 0$) |
|-----------------------|-----------|------------|-----------------|-----------|---------|---------------------------------|---------|---------------------------------|--------------------|--------------------------------------------|
| 1.30 | 15.9 | 0.684 | 0.0966 | 0.0534 | 0.48 | 0.50 | 0.084 | 0.088 | 1.10 | 1.10 |
| 1.30 | 17.5 | 0.734 | 0.0934 | 0.0487 | 0.54 | 0.57 | 0.096 | 0.101 | 1.12 | 1.13 |
| 1.38 | 17.9 | 0.716 | 0.0900 | 0.0475 | 0.52 | 0.54 | 0.086 | 0.090 | 1.10 | 1.10 |
| 1.41 | 18.5 | 0.623 | 0.0740 | 0.0459 | 0.52 | 0.55 | 0.082 | 0.086 | 1.07 | 1.08 |
| 1.41 | 20.0 | 0.378 | 0.0460 | 0.0426 | 0.54 | 0.56 | 0.064 | 0.067 | 1.03 | 1.03 |
| 1.42 | 20.8 | 0.204 | 0.0143 | 0.0410 | 0.54 | 0.56 | 0.034 | 0.035 | 1.00 | 1.00 |
| 1.42 | 20.7 | 0.105 | 0.0070 | 0.0411 | 0.55 | 0.57 | 0.031 | 0.032 | 1.02 | 1.02 |
| 1.42 | 21.1 | 0.045 | 0.0018 | 0.0404 | 0.57 | 0.60 | 0.014 | 0.015 | 1.01 | 1.00 |
| 1.42 | 20.8 | 0.022 | 0.0009 | 0.0409 | 0.56 | 0.59 | 0.013 | 0.014 | 1.03 | 1.03 |
| 1.42 | 20.4 | 0.012 | 0.0004 | 0.0418 | 0.63 | 0.65 | 0.011 | 0.011 | 1.02 | 1.02 |
| 2.86 | 16.2 | 0.602 | 0.2238 | 0.0526 | 0.28 | 0.29 | 0.057 | 0.060 | 1.09 | 1.09 |
| 2.84 | 17.4 | 0.472 | 0.1212 | 0.0489 | 0.27 | 0.28 | 0.050 | 0.052 | 1.04 | 1.04 |
| 2.84 | 19.7 | 0.259 | 0.0567 | 0.0431 | 0.30 | 0.31 | 0.040 | 0.042 | 1.02 | 1.02 |
| 2.82 | 20.6 | 0.127 | 0.0234 | 0.0413 | 0.30 | 0.31 | 0.034 | 0.035 | 1.00 | 1.00 |
| 2.82 | 20.6 | 0.058 | 0.0081 | 0.0413 | 0.30 | 0.31 | 0.026 | 0.027 | 1.00 | 1.00 |
| 2.82 | 20.5 | 0.025 | 0.0034 | 0.0415 | 0.34 | 0.35 | 0.024 | 0.025 | 1.00 | 1.00 |
| 2.82 | 20.7 | 0.011 | 0.0016 | 0.0411 | 0.34 | 0.35 | 0.023 | 0.024 | 1.02 | 1.02 |
| 2.82 | 20.3 | 0.008 | 0.0009 | 0.0420 | 0.36 | 0.37 | 0.005 | 0.005 | 1.01 | 1.01 |
| 0.20 | 13.0 | 0.694 | 0.0336 | 0.0652 | 0.94 | 1.00 | 0.131 | 0.140 | 1.02 | 1.02 |
| 0.55 | 12.5 | 0.700 | 0.0524 | 0.0681 | 0.73 | 0.78 | 0.108 | 0.115 | 1.09 | 1.09 |
| 0.90 | 11.9 | 0.656 | 0.0686 | 0.0716 | 0.55 | 0.59 | 0.084 | 0.090 | 1.13 | 1.13 |
| 1.58 | 11.9 | 0.568 | 0.1045 | 0.0715 | 0.33 | 0.35 | 0.054 | 0.058 | 1.06 | 1.06 |
| 2.46 | 12.1 | 0.459 | 0.1486 | 0.0703 | 0.22 | 0.23 | 0.044 | 0.047 | 1.02 | 1.02 |
| 3.54 | 11.7 | 0.481 | 0.1521 | 0.0728 | 0.14 | 0.15 | 0.029 | 0.031 | 1.03 | 1.03 |
| 5.35 | 10.9 | 0.449 | 0.2076 | 0.0780 | 0.09 | 0.10 | 0.023 | 0.025 | 1.02 | 1.02 |

Table 1. Table of Experimental Data (Continued)

| $\frac{\omega}{2\pi}$ | \bar{U} | ϵ | $\epsilon C_2 $ | β_0 | $ D_1 $ | $ D_1 $ ($\beta_0 \neq 0$) | $ D_2 $ | $ D_2 $ ($\beta_0 \neq 0$) | $1 + \bar{\sigma}$ | $1 + \bar{\sigma}$ ($\beta_0 \neq 0$) |
|-----------------------|-----------|------------|-----------------|-----------|---------|---------------------------------|---------|---------------------------------|--------------------|--------------------------------------------|
| 2.18 | 10.8 | 0.263 | 0.0421 | 0.0789 | 0.23 | 0.25 | 0.029 | 0.031 | 1.04 | 1.03 |
| 2.37 | 11.3 | 0.168 | 0.0251 | 0.0752 | 0.21 | 0.23 | 0.023 | 0.025 | 1.04 | 1.04 |
| 2.52 | 11.9 | 0.076 | 0.0094 | 0.0712 | 0.21 | 0.23 | 0.015 | 0.016 | 1.04 | 1.03 |
| 2.44 | 11.6 | 0.120 | 0.0155 | 0.0737 | 0.22 | 0.23 | 0.018 | 0.019 | 1.04 | 1.04 |
| 2.58 | 12.1 | 0.052 | 0.0056 | 0.0702 | 0.22 | 0.24 | 0.014 | 0.015 | 1.05 | 1.04 |
| 0.96 | 4.3 | 0.323 | 0.0793 | 0.1962 | 0.22 | 0.26 | 0.034 | 0.041 | 1.03 | 1.00 |
| 2.54 | 17.8 | 0.614 | 0.1240 | 0.0478 | 0.30 | 0.31 | 0.018 | 0.019 | 1.10 | 1.11 |
| 1.36 | 18.1 | 0.538 | 0.0796 | 0.0470 | 0.54 | 0.57 | 0.036 | 0.038 | 1.07 | 1.08 |
| 0.84 | 17.9 | 0.563 | 0.0525 | 0.0474 | 0.69 | 0.72 | 0.030 | 0.031 | 1.07 | 1.07 |
| 0.36 | 17.9 | 0.532 | 0.0576 | 0.0475 | 0.92 | 0.97 | 0.050 | 0.052 | 1.04 | 1.04 |
| 3.20 | 11.5 | 0.428 | 0.0727 | 0.0737 | 0.17 | 0.18 | 0.025 | 0.027 | 1.02 | 1.02 |
| 1.80 | 11.5 | 0.369 | 0.0598 | 0.0737 | 0.29 | 0.31 | 0.043 | 0.046 | 1.02 | 1.02 |
| 5.05 | 11.1 | 0.508 | 0.1367 | 0.0770 | 0.11 | 0.12 | 0.017 | 0.018 | 1.06 | 1.06 |
| 9.90 | 10.6 | 0.476 | 0.0293 | 0.0801 | 0.05 | 0.06 | 0.003 | 0.003 | 1.03 | 1.02 |

| | | | | |
|----------------------------------------------------------------------------------------------------------------------------------------------------------------------------------------------------------------------------------------------------------------------------------------------------------------------------------------------------------------------------------------------------------------------------------------------------------------------------------------------------------------------------------------------------------------------------------------------------------------------------------------------------------------------------------|--|---------------------------------------------------------|-----------------------------------------------------|------------------------------|
| U.S. DEPT. OF COMM. BIBLIOGRAPHIC DATA SHEET | | 1. PUBLICATION OR REPORT NO. NBSIR 75-772 | 2. Gov't Accession No. | 3. Recipient's Accession No. |
| 4. TITLE AND SUBTITLE THE DYNAMIC RESPONSE OF HELICOID ANEMOMETERS | | | 5. Publication Date November 1975 | |
| | | | 6. Performing Organization Code | |
| 7. AUTHOR(S) James M. McMichael and Philip S. Klebanoff | | | 8. Performing Organ. Report No. NBSIR 75-772 | |
| 9. PERFORMING ORGANIZATION NAME AND ADDRESS NATIONAL BUREAU OF STANDARDS DEPARTMENT OF COMMERCE WASHINGTON, D.C. 20234 | | | 10. Project/Task/Work Unit No. 2130482 | |
| | | | 11. Contract/Grant No. 1-1-1377 | |
| 12. Sponsoring Organization Name and Complete Address (Street, City, State, ZIP) Federal Highway Administration (DoT) Office of Research Structures and Applied Mechanics Division Washington, D. C. 20590 | | | 13. Type of Report & Period Covered Final | |
| | | | 14. Sponsoring Agency Code | |
| 15. SUPPLEMENTARY NOTES | | | | |
| 16. ABSTRACT (A 200-word or less factual summary of most significant information. If document includes a significant bibliography or literature survey, mention it here.) The results of an analytical and experimental investigation of the dynamic response of a helicoid anemometer are presented. The experimental investigation was conducted using the NBS Unsteady Flow Facility and data are presented which illustrate the dynamic behavior in a spatially uniform, fluctuating flow with varying amplitudes, frequencies, and mean velocities. An analytical model governing the dynamic response is also presented and compared with the experimental results. | | | | |
| 17. KEY WORDS (six to twelve entries; alphabetical order; capitalize only the first letter of the first key word unless a proper name; separated by semicolons) Air; analytical; anemometer; dynamic response; experimental; lag; unsteady flow. | | | | |
| 18. AVAILABILITY <input checked="" type="checkbox"/> Unlimited <input type="checkbox"/> For Official Distribution. Do Not Release to NTIS <input type="checkbox"/> Order From Sup. of Doc., U.S. Government Printing Office Washington, D.C. 20402, SD Cat. No. C13 <input checked="" type="checkbox"/> Order From National Technical Information Service (NTIS) Springfield, Virginia 22151 | | 19. SECURITY CLASS (THIS REPORT) UNCLASSIFIED | | 21. NO. OF PAGES 53 |
| | | 20. SECURITY CLASS (THIS PAGE) UNCLASSIFIED | | 22. Price \$ 4.25 |

